[Catégorie]

PolarMonitoring WP3: Simulation and Performance Analysis

Reference:	CLS-ENV-NT-20-0064
Nomenclature:	[Nomenclature]
Issue:	1. 1
Date:	2020,Feb.19

CLS headquarters
11 rue Hermès
Parc technologique du Canal
31520 Ramonville Saint-Agne
FRANCE

Tel. +33 (0)5 61 39 47 00
Fax +33 (0)5 61 75 10 14
Mail: info@cls.fr
www.cls.fr

CLS Brest Le Ponant
Zone du technopôle de Brest Iroise
Avenue La Pérouse
29280 Plouzané
FRANCE

Tel. 33 (0)2.98.05.76.80
Fax 33 (0)2.98.05.76.90

Chronology Issues:

Issue:	Date:	Reason for change:	Author
1.0	14/02/2020	Initial version	F.Larue ; G.Picard ; J.Aublanc ; P.Thibaut
1.1	19/02/2020	Conclusion + minor revisions	F.Larue ; G.Picard ; J.Aublanc ; P.Thibaut

People involved in this issue:

Written by (*):	F.Larue G.Picard J.Aublanc	Date + Initials:(visa or ref) 
Checked by (*):	P.Thibaut	Date + Initial:(visa ou ref) [Checker]
Approved by (*):		Date + Initial:(visa ou ref) [Approver]
Application authorized by (*):		Date + Initial:(visa ou ref)

In the opposite box: Last and First name of the person + company if different from CLS

Index Sheet:

Context:	
Keywords:	[Mots clés]
Hyperlink:	

Distribution:

Company	Means of distribution	Names
CLS	Notification	

List of tables and figures

List of tables:

List of figures:

Reference documents

RD 1 Manuel du processus Documentation
CLS-DOC

List of Contents

1. Introduction

Radar altimeter waves are known to be affected by signal penetration and subsurface scattering into snow and ice [Ridley and Partington, 1988]. The mechanisms for radar-altimeter scattering are still poorly known, which is a major issue when attempting to measure the surface elevation over ice sheets and sea-ice floes. As a result, the backscattered altimeter signal is a complex combination of energy backscattered from the surface and the subsurface, with contributions that may vary significantly in space and time depending on the density, the temperature, the stratification and the grain size of the snowpack [Partington et al., 1989; Legresy and Remy, 1998; Lacroix et al., 2008; Remy et al., 2012]. Over the ice sheets, radar altimeter measurements are additionally influenced by the slope and surface roughness (from centimeter to meter scales, as for sastrugi and snow megadunes), making the surface elevation estimation even more difficult.

With respect to Ku-band, Ka-band radar altimeter is much more reliable for providing consistent measurements of the surface. Indeed Ka-band waveforms are not, or only weakly, impacted on their leading edge by volume scattering because of a penetration depth lower than in Ku-band, which is well known in theory. At present, no single technique makes it possible to inform about the snowpack properties, and even less about the snow depth over snow covered surfaces. But by combining dual-frequency (Ku and Ka having different snow volume signals) backscattering measurements, it is expected to find a number of features linked to snow parameters that would allow to characterize the subsurface and possibly to retrieve geophysical information on snow extent and snow depth on both land and sea ice.

This study aims at providing some answers about the potential benefits of a dual Ku/Ka band instrument for snow measurements. For that purpose, the first objective is to develop a dedicated numerical simulator, able to generate synthetic CRISTAL Ku/Ka waveforms, in both LRM and SAR modes, and over different types of snowpack. The simulator is developed in synergy between IGE and CLS. IGE providing their expertise in glaciology, along with the Snow Model Radiative Transfer [Picard et al., 2018]. CLS providing their expertise in altimetry, along with AltiDop, an extensively used altimetry simulator, currently used for oceanic and hydrologic studies.

The second objective is to use the simulator to study radar altimetry over ice sheets and sea ice surfaces, in the CRISTAL dual bands altimeter configuration. Over ice sheet, the plan is to apply it to Vostok area, well known from different studies because of the flatness of the surface due to the underground lake. The altimetry sensitivity to snow parameters and surface slope is assessed. The benefits of the dual Ku/Ka bands are analysed, especially its capacity to characterize the snowpack properties, and at the end, providing estimations of surface elevation.

2. SMRT adaptations to altimetry

2.1. SMRT presentation

The simulation of the total backscatter signal from a snow-cover surface has been addressed by many research groups, not only for the traditional nadir altimetric radar, but also for the side looking scatterometers and SAR. As detailed by Cui et al. (2016), the total backscattering over snowpack covering sea ice or ice sheet at a given incident angle is the sum of the surface scattering component from air-snow interface (σ_{surf}), a volume scattering component from snowpack (σ_{vol}), the interaction component between snow volume and snow-ice interface, and the direct subsurface scattering component. A common approach is to simulate the backscattering coefficient from snowpack (σ_{vol} with an electromagnetic scattering model, and the surface backscattering component with a surface model adequate to the roughness scales (σ_{surf}, including scattering at air-snow and snow-ice interfaces).

Basically, in electromagnetic scattering models, propagation parameters of the snowpack are estimated first (extinction coefficients, scattering phase matrix and the effective propagation constant), and used to solve the radiative transfer equation in order to compute the total backscattering coefficient in a second step. To estimate the propagation parameters of the snowpack, snow must be considered as a dense media (as opposed to other media that are sparse, such as the vegetation). Dense media affect both the propagation (absorption and speed) in the medium (at any frequency) and short range multiple scattering between the scatterers (at high frequencies). Several approaches exist to represent the snowpack as a dense media: Snow can be considered as a dense random collection of discrete particles described by the Quasi-Crystalline Approximation (QCA, Tsang et al., 2007) or the Improved Born Approximation (Matzler, 1987). Figure 1 illustrates the snowpack representation with the QCA approximation.

With QCA-based models, snow is often represented with spherical particles randomly distributed in space (spheroids can be used as well). In these cases, snow scattering properties depend on density, particle size and shape of each snow layer. With IBA, snow is represented as a collection of scatterers for the polarizability calculation but is represented by geometrical statistics of the ice matrix for the scattering calculation. This dual representation, albeit inherently incompatible in theory, has practical advantages as recent work has shown that snow microstructure is not well represented by scatterers with a single shape and size. In the original formulation of IBA (Matlzer 1987), a collection of independent spheres was considered, which proved to be unrealistic for snow. The initial practical implementation of IBA in the MEMLS snow model used the exponential autocorrelation function to represent snow microstructure which became very popular. New evidence (unpublished) shows that this is not a perfect representation and that distribution with two parameters (one controlling the small-scale/grain size and one controlling the large scale/grain arrangement) is more efficient.

The quasi-equivalence of IBA and QCA was recently demonstrated by Löwe and Picard (2015) when the autocorrelation function of IBA is adapted to match the sticky hard sphere description used in QCA-base models showing that the electromagnetic model (either QCA or IBA) is much less critical than the choice of the microstructure description. This key result motivated the development of SMRT, with the capability to switch between different microstructure representation.

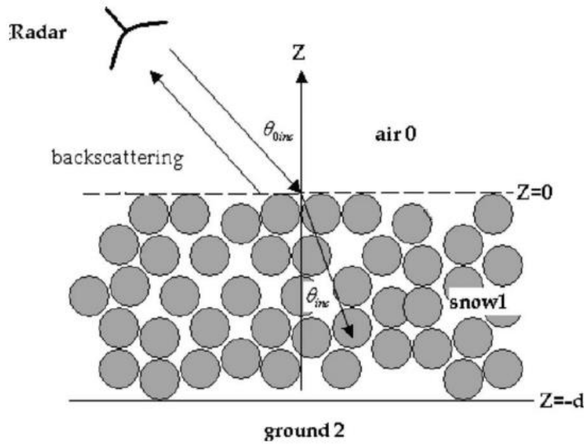

Figure 1:Active microwave remote sensing by Tsang et al. (2007). Snow is represented as a dense media with the QCA approximation.

Once the snow propagation and scattering properties in each layer are calculated, the propagation through the different layers of the snowpack and the inter-layer multiple scattering are solved using the radiative transfer theory numerically (Tsang et al., 2007; Xu et al., 2012). Longepe et al. (2009) initially developed an active microwave model based on the DMRT-QCA theory but included only single inter-layer scattering mechanisms (though inter grain scattering was taken into account through the QCA model). Several active microwave radiative transfer models were adapted later for multiple scattering to simulate total backscattering coefficient from a multi-layered snowpack (DMRT-QMS based on QCA, MEMLS based on IBA, etc.) in various angular and polarimetric configurations (Tsang et al., 2007; Liang et al., 2008a, 2008b; Song et al., 2012; Proksch et al., 2015). These models are particularly adapted for high-frequency radar (Ku band and higher frequencies) because they accont for multiple scattering. Nevertheless, these models use the time-independent radiative transfer equation, they are not adapted for altimetric applications.

Numerous models exist due to the large number of possible approaches to estimate each parameter (effective snow permittivity, scattering, radiative transfer equation, etc.), and the wide range of applications. All have shown consistency with measured data in the past (e.g. Picard et al., 2018). A small subset, the most generic models, are well known and widely shared in the snow microwave community, especially for passive microwaves.

The large number and diversity of existing models make it difficult to choose the most suitable model. This fact further motivated Picard et al. (2018) to develop the Snow Microwave Radiative Transfer (SMRT) model in the framework of the ESA project “Microstructural origin of electromagnetic signatures in microwave remote sensing of snow”, starting in 2015. SMRT also computes the total backscatter model of snowpack in the microwave domain in addition to the thermal emission (Picard et al., 2018). More precisely, the targeted validity is in the range 1-200 GHz, but not all the components are fully valid in the highest frequencies yet. For most snowpacks, the validity should be reasonable at S, Ku and Ka bands, which is relevant for this study. Compared to existing models such as MEMLS or DMRT-QMS, SMRT was developed to unify and inter-compare different descriptions of the snow microstructure found in different microwave models. For that, SMRT offers the capability of switching between different electromagnetic theories, representations of snow microstructure, and other modules involved in various calculation steps. The current version of SMRT includes the Dense Media Radiative Transfer theory (DMRT, Tsang et al., 1985), the Improved Born Approximation (IBA, Mätzler, 1998), independent Rayleigh scatterers and the Strong Fluctuation theory (Tsang et al., 2007) to compute the intrinsic electromagnetic properties of snow layers. Under IBA, SMRT is able to use different microstructure representations of snow (or any bi-phase media). SMRT is driven with:

- snowpack properties (thickness, density, temperature and snow grain size, liquid water content for each layer),
- properties of the underlying surface (type of materials, roughness, wetness, salinity, etc.),
- characteristics of the sensor (active or passive, frequency, polarization, incidence angle).

In the active configuration, SMRT simulates the total backscattering coefficient at a given polarization and incidence angle (σ_{surf} and σ_{vol}).

SMRT is written in Python, clearly structured and modular, allowing easy inter-comparisons between different modelling approaches.

SMRT has been extended to work on sea-ice and lake-ice in 2018 by a group of sea-ice scientists and by the initial SMRT developers. For this, ice layers have been added. These layers may contain either air bubbles or brine pockets but cannot contain both; at least not yet. Nevertheless, this enables modelling lake ice as "fresh ice with air bubbles", first year sea-ice as "weakly-saline ice with brine pockets" and multiyear ice as "saline ice with air bubbles". In addition, a parameterization for saline snow has been added. The extension was technically easy thanks to the modularization of the model components, but the evaluation of the performance for terrestrial snowpack and even more for sea-ice, is a slowly progressing work. Despite the initial focus of this extension being SMOS, scattering and propagation formulations are thought to be valid for the same range as for snow, i.e.1-100 GHz.

The implemented radiative solver of SMRT was time-independent, and at this stage, SMRT was not yet adapted for simulating altimetric waveforms.

2.2. Adaptation for altimetric applications

The altimetric waveform is the backscattered power measured at the satellite as a function of the time from the emission of a pulse of microwaves (Figure 2).

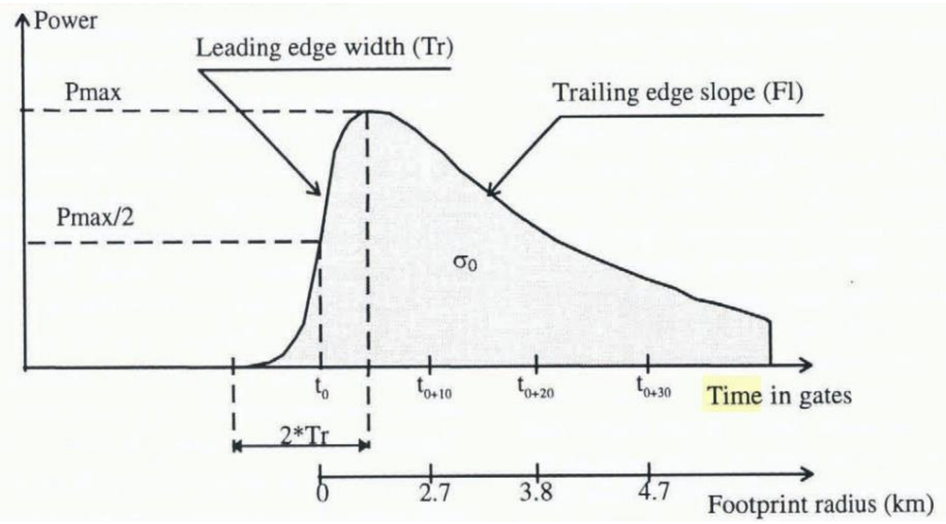

Figure 2: Waveform parameters description, by Legresy and Remy (1997).

Formulations for the surface backscatter (oceanic surface) has been proposed by Brown (1977), who showed that the received signal is the convolution of 1) the emitted pulse signal 2) the return delay due to surface height variations (roughness) around the mean surface and 3) a time function (PFS) accounting for the progressive return within the footprint, from the center (at nadir) to the side of the footprint. For the latter function, it is also possible to account for the variation of the surface backscatter with the incidence angle – that despite the very small variations of the incidence angle (0-2° typically) the influence is notable for smooth surfaces, such as snow – and to account for the curvature of the Earth. The PFS proposed by Brown formally writes:

$$P_{\mathrm{FS}}(t) = \frac{\lambda^2}{(4\pi)^3} \int_S \frac{\delta\left(t - \frac{2r}{c}\right)\sigma_s^0(\theta) G^2(\theta)}{r^4} dS \quad [1],$$

where G is the antenna known and σs (also called sigma naught) the surface backscatter. r is the distance from the surface to the satellite. Brown (1977) developed this equation in the case the antenna pattern is an exponentially decreasing function of the angle.

where G is the antenna gain and σs (also called sigma naught) the surface backscatter. r is the distance from the surface to the satellite. Brown (1977) expanded this equation when the antenna pattern is an exponentially decreasing function of the angle.

For penetrable media such as snow and ice, the signal has an additional component, called "volume" in the altimetry community, because it comes after (below) the surface, but based on the nomenclature used by 1st order radar modelers, this component indeed includes volume scattering and backscatter from the snowpack internal interfaces. This component is convoluted with the other components (see 1, 2, 3).

This theory is in principle adequate when the dominant reflection of energy comes from the snow-ice interface and to build the radar echo received by the satellite by neglecting the snow-air interface and volume scattering (Kurtz et al., 2014; Davis et al., 2017). Nevertheless, this assumption is not realistic when the snow cover contains wet or saline layers, which is the case for snow cover over sea ice, or for deep snow as on the ice sheets.

Newkrik and Brown (1996) and Adams and Brown (1998) proposed rigorous formulations for penetrable media, based on the time-dependent radiative transfer equation (Tossendorf, 1989) in order to account for the time-travel of the wave (propagation speed) in the snowpack. However, their derivation focuses on the delay due to volume scattering considering a generic backscatter function as a function of depth, not on a precise description of the medium. A practical use of their theory requires an adequate (and precise) backscatter model for the medium under consideration (for the volume and for the interfaces). A few studies created a waveform simulator for ice sheet backscatter by converting the total backscattering simulated for a single layer snowpack (Ridley and Partington, 1988) or for a multi-layer snowpack (Legrésy and Rémy, 1997) to the backscattered power as a function of time using loss factor to account for the extinction of the wave in the snowpack, first order theory and time travel based on geometrical consideration. Nevertheless, they used simplified analytical equations to estimate volume scattering, and not a detailed radiative transfer model (Rémy, 2012). Tonboe et al. (2006a) used the MEMLS multilayer radiative transfer model to simulate scattering and extinction for each layer (σ_{vol} under Improve Born Approximative, IBA, Mätzler, 1998), and an empirical reflection formulation (close to geometrical optics) for the surface (Fetterer et al., 1992), but they neglected the internal interfaces.

From these pioneering studies and implementation, Lacroix et al. (2008) built a model for the ice-sheets, using the Improve Born Approximative for the volume, and the Integral Equation Model (IEM, Fung et al. 1992) for the surface and interfaces. Both approximations have proved their performance, and their validity range is relatively well established. Lacroix' model is a first order model, that is, it only computes single scattering. For the propagation of the wave, it uses the result of Adams and Brown (1998) to adapt the Brown model to a multi-layered snowpack. Briefly, under the small angle approximation, all the paths in the snow are along the z-axis (the off-nadir is small: ~1°). The PFS of a buried interface is thus similar to the PFS of the surface except that backscattering properties are different (attenuated by the snow medium), and the PFS is shifted in time by the vertical time travel in the snow, which depends on the vertical profile of refraction index (or equivalently speed of light in the medium). In other words, the sub-surface model is the convolution of the PFS and the vertical distribution of the scattering properties of the medium. The surface contribution depends on the

FORM-NT-GB-7-1

snow density heterogeneity and roughness features, and the volume contribution depends of scattering by snow grains, i.e of snow grain size. Hence, the 'flat volume' impulse response of a multi-layered snowpack is written as follows (Lacroix et al., 2008):

$$P_{\mathrm{FV}}(t) = \frac{1}{(4\pi)^3 H^4}\left[P_{\mathrm{layers}} + P_{\mathrm{grains}}\right]$$

$$P_{\mathrm{layers}}(t) = \sum_{n=1}^{N} \lambda_n^2 \cdot A(z_n) \cdot \delta(t - t_{\mathrm{v}}(z = z_n))$$

$$\otimes \int_S \delta(t - t'(z=0,\theta))\sigma_1^0(z = z_n, \theta) G^2(\theta) dS$$

$$P_{\mathrm{grains}}(t) = \int_z \lambda^2(z) \cdot A(z) \cdot \delta(t - t_v(z))\gamma_{\mathrm{grains}}(z) dz$$

$$\otimes \int_S \delta(t - t'(z=0,\theta)) G^2(\theta) dS \quad [2],$$

with A(z) the extinction at the depth z, N is the number of internal layers, λn is the radar wavelength at the depth of the layer n, zn. dz is computed considering the dielectric properties of the medium. Lacroix's model is a computer code in matlab. The surface scattering are estimated by considering small scale roughness with the IEM model (detailed in the next Section). The IEM part is coded in Fortran.

2.3. Developments

2.3.1. Adaptation of SMRT for radar altimetry

The review showed that several altimetric models have been developed, with all having some identifiable limitations. The most stringent issue is that they are not widely available, so not widely used and as a consequence are not well validated. They also are somewhat incomplete, because the authors have made a series of fixed/hard coded choices (theories, assumptions, …) for the many different components, which may be relevant for their specific application but makes such models difficult to apply in other conditions. It results that their usability is very low.

SMRT was built from 2015 with the aim to make available the existing diversity of modelling work (of historical interest only for some of them) in a unique code base, accessible to a wide public, with the hope: 1) to promote validation and contribution by the community, and 2) to facilitate future implementations of models by building on existing, solid, components instead of re-building all the components every time. The adaptation of SMRT to radar altimetry follows this same strategy and really benefits for it. The only necessary addition is the time-dependent radiative transfer solver needed for the altimetry, almost all the other components for media (snow, ice, sea-ice), volume and interface scattering theories, etc are already available in SMRT, well tested.

The new "nadir_altimetry" solver in SMRT follows Lacroix et al. (2008) and Adams and Brown (1998). Once the medium is defined by the user, and scattering and propagation properties for each layer and interfaces are calculated using the existing SMRT modules (see Picard et al. 2018), the "nadir_altimetry" solver aims at solving the propagation in the air and in the medium of the wave over the footprint area. Lacroix et al. 2008 and Adams and Brown 1998 demonstrate that this can be achieved in two independent steps: 1) the propagation in the medium, from the surface to the internal layers, 2) the propagation in the air from the altimeter to the surface (and back). The second step corresponds to the calculation of the PFS, and is a solved problem since Brown 1977. It is also already implemented in AltiDop with many more details (ie. less restrictive assumptions) than in Brown 1977, enabling to take into account the subtleties of the sensors and terrain topography. SMRT implements the Brown model as a side product of this project, enabling to produce waveforms for a horizontal surface.

The main task addressed in this work package is the first step. As detailed in Adams and Brown, 1998, or by Lacroix et al. 2008, the goal is to solve the equation of the time-dependent radiative transfer for a wave incoming at the surface of the medium. The equation writes:

$$\begin{aligned}\frac{1}{c(\mathbf{r})}\frac{\partial}{\partial t}I'(\theta,\phi,\mathbf{r},t)+\frac{\partial}{\partial s}I'(\theta,\phi,\mathbf{r},t) = \\ -\kappa_e(\mathbf{r})I'(\theta,\phi,\mathbf{r},t) \\ +\frac{1}{4\pi}\int_{4\pi}P(\theta,\theta',\phi-\phi',\mathbf{r})I'(\theta,\phi,',\mathbf{r},t)d\Omega'\end{aligned} \quad [3],$$

where I' is the reduced specific intensity of the wave (the unknown). c the speed of light, P the phase matrix and Ke the extinction coefficient. They are the parameters describing the medium and are obtained from SMRT existing code (electromagnetic model) for every layer (made of fresh or saline snow, fresh, saline and bubbly ice,...). The iterative method is a well-known method (Tsang et al. 2001) to solve the time-independent equation when scattering is weak with respect to absorption (which is valid for most snow up to Ku), that is the equation where the first term is removed. This method similarly applies when the time dependence is included. The 0th order is obtained by neglecting the scattering term (the integrale with the phase matrix) and has the form of a downwelling wave, with exponentially decreasing intensity, attenuated by interface transmittances T and with a time delay controlled by the path and speed of light in the medium:

$$\begin{aligned}I^{0^{\text{th}}}(\theta,z,t) = E_0\left(t-\int_0^z\frac{dz}{c(z)}\right)\delta(\cos\theta_0) \\ \exp\left(-\int_0^z\kappa_e(z)dz\right)\prod_{i=0}^{N(z)}T_i(z)\end{aligned} \quad [4],$$

where Eo is the incident intensity pulse at the surface. The equation is valid for any near-nadir direction θ_0. Injecting this 0th order solution in the scattering term of the equation and solving it for the nadir direction (θ_0=0) yields the 1st order solution:

$$\begin{aligned}I^{1^{\text{st}}\text{ vol.}}(z=0,t) = \int_{z=0}^{H}dz\ E_0\left(t-2\int_{z=0}^{z}\frac{dz'}{c(z')}\right) \\ \frac{1}{n^2(z)}\frac{P(0,0,\pi,z)}{4\pi} \\ \exp\left(-2\int_0^z\kappa_e(z')dz'\right)\prod_{i=0}^{N(z)}T_i^2\end{aligned} \quad [5].$$

This equation is easier to understand that it looks at first sight. The 1th order backscattering from the volume (i.e. the snow grains or air bubbles in air) is the vertical integral over the medium of the local backscatter (the term with the phase matrix P), attenuated from the surface to depth z with

FORM-NT-GB-7-1

the extinction Ke (the exponential term) and attenuated by the two-way transmission at each interface T². The two-way delay is in the Eo term.

The integrals in the equation are in practice converted into a discrete sum, accounting for the homogeneity of all the parameters (c, Ke and P) within each layer and neglecting the time travel difference within a layer (which can be true by splitting homogeneous layer in thinner sublayers until this condition becomes valid). The backscatter from layer j is

$$I_j^{1^{\mathrm{st}}\,\mathrm{vol.}}(z=0,t) = E_0\left(t-2\sum_{j'=0}^{j-1}\frac{h_{j'}}{c(z_{j'})}\right)$$
$$\frac{1}{n(z_j)}\frac{P(0,0,\pi,z_j)}{4\pi}\frac{1-\exp\left(-2\kappa_{\mathrm{e}}h_j\right)}{\kappa_{\mathrm{e}}(z_j)}$$
$$\exp\left(-2\sum_{j'=0}^{j-1}\kappa_{\mathrm{e}}(z_{j'})h_{j'}\right)\prod_{i=0}^{N(z_j)}T_i^2. \quad [6],$$

where h is the thickness of each layer. The first line controls the time delay, the second is the 1st order backscatter of the homogeneous layer (e.g. Picard, 2002) and the last line controls the attenuation.

Similarly, the backscatter from the interface j (surface and inter-layer interfaces) is derived, following the very same approach:

$$I_j^{1^{\mathrm{st}}\,\mathrm{int.}}(z=0,\theta_0,t) = E_0\left(t-2\sum_{j'=0}^{j-1}\frac{h_{j'}}{c(z_{j'})}\right)$$
$$\frac{1}{n(z_{j-1})}\frac{\sigma^0(\theta_0,z_j)}{4\pi}\frac{1-\exp\left(-2\kappa_{\mathrm{e}}h_j\right)}{\kappa_{\mathrm{e}}(z_j)}$$
$$\exp\left(-2\sum_{j'=0}^{j-1}\kappa_{\mathrm{e}}(z_{j'})h_{j'}\right)\prod_{i=0}^{N(z_j)}T_i^2. \quad [7].$$

SMRT computes the sum of volume and interfaces, and optionally the three backscatter components independently. This option is useful to investigate the contributions of the different mechanism to the waveform: volume, surface and internal interfaces. It is also needed by AltiDop to perform its computation.

Practical implementation.

The implementation consists in two additional files:

altimeter_list.py is dedicated to altimeter characteristics. It contains the antenna pattern and the analytical equation of the corresponding PFS, proposed by Brown et al. 1977 (we also implemented the Newkrik and Brown 1992 model, but it is not useful for space-borne altimetry sensor and it is not used at all in the following). Second, it contains the sensor parameters (e.g. central frequency, beamwidth, bandwidth, altitude et # of gates) for Envisat, Sentinel 3 and Saral-AltiKa at the time of writing but aimed at being extended. Note that this file will be probably split in two files: antenna_pattern.py and altimeter_list.py when transferred to the official SMRT repositories to separate the easily extendable file (altimeter_list.py) from the less user friendly one (antenna_pattern.py)

nadir_altimetry.py is a radiative transfer (RT) solver (in SMRT wording), as DORT, except that the result is the time-dependent backscatter (i.e. the waveform) instead of being total backscatter. The method "solve" is the entry point (as for any SMRT RT solver) and is internally called when the SMRT user uses Model.run. AltiDop directly uses this entry point. "solve" first calls "vertical_scattering_distribution", which implements the 1st order equations described in the previous section, and returns the backscatter as a function of time for the volume, surface and interface. "Solve" then optionally performs the convolution of these three signals with the PFS (the Brown model) and the altimeter pulse to obtain the waveform (or the three components of it). The convolution step can be opt-out, which is used for the SMRT-AltiDop coupling to perform the PFS AltiDop (more complex) convolution. SMRT currently neglects the time spread due to the surface roughness (it accounts for the backscatter from the rough surface but not the time spread due to the difference of height of the surface).

Apart from these two files, only minor changes were required in the remaining of the SMRT code base and none of them introduced backward incompatibilities.

2.3.2. Implementation of two surface scattering models

At the beginning of this project, SMRT had no suitable surface scattering model or radar backscatter computation. SMRT only had flat surface/Fresnel theory (which has no backscatter), empirical rough surface model dedicated to passive microwave (e.g. Wegmuller and Matzler's or QNH models) and on ad hoc model where the backscatter value is prescribed, not calculated with a physical model.

The growing interest of SMRT as an active model, for altimetry or side looking radars, motivated us to implement two new physically-based rough surface models: geometrical optics (GO) model (commonly used for ocean surface, i.e large scale roughness) and the IEM model (commonly used for soil, i.e small scale roughness).

Both present an interest for snow-cover areas. GO is suitable for the surface (and internal interfaces) roughness, which often has meter-scale dunes (e.g. sastrugi). IEM is suitable for the soil under the snowpack, and maybe as well for small-scale surface roughness features (e.g. ripples, hoar). IEM was also used in Lacroix 2008, and was therefore needed for the inter-validation.

IEM is adapted for moderate roughness (with respect to the wavelength), and more precisely for k.σr < 3 and kσr.kl < sqrt(eps), with k the wavenumber. In Ku band, it implies surface height rms (σr) < 10 cm, and < 5 cm in Ka band. The implementation faithfully follows the original publication of Fung et al. (1992) and has been validated with the Fortran version in Lacroix et al. 2008. It also asymptotically gives the same results as the Kirchoff approximation (also known as physical optics). Further checks may be necessary. An important limitation is that IEM, as published in 1992, is only for the backscatter direction, it does not calculate the full bi-direction reflectance function. Multiple scattering between the snowpack and the substrate (or between interfaces) can not be accounted for with this model. This limits the use to low frequencies when 1st order is sufficient. As this approximation has also been necessary for the nadir_altimetry implementation, the current limitation of IEM is not a bottleneck for the present study. Implementing the full bi-directional advanced IEM (AIEM) is a perspective.

The Geometrical Optics approximation is adapted for large surface roughness height k.σr > 3 which applies to all the large scale objects we can see on the snow surface after a wind event (dunes, sastrugi, ...). This model features no frequency dependence as a consequence of the large k.σr assumption. The implementation is proposed in two versions following Tsang et al. (2001), the first one only has the backscatter direction and has a simple, readable, and computationally efficient expression, while the second is for the full bi-directional reflectance. As explained for IEM, the nadir_altimetry model can use the first one without additional constraints.

2.3.3. Normalisation with a radar calibration sphere

SMRT nadir_altimetry module computes the power received by the altimeter, which is not directly related to the backscattering coefficient as a function of time. This signal depends on parameter from the satellite (e.g. pulse duration, altitude). Instead of tracing back the right calibration constant in the theory (which varies between theory and can be quite complex to do so), we decided to mimic the process used with real altimetric observations. The calibration is based on relating the signal of the surface of interest to the signal of a surface with known sigma naught ('σs').

For this, we implemented in SMRT a surface with an ideal isotropic backscatter of value 4π, which is in principle how sigma naught is defined. This simple addition allows us to perform the "calibration" of the numerical PFS implemented for each sensor, and thus to compute the total backscattering coefficient. This is useful for the comparison with the output of the DORT code, and thereby assess the relative importance of the 1st order scattering vs higher order scattering.

Another way to compute the total backscattering coefficient, as well as the other altimetric parameters, is to apply a retracking algorithm on the waveform (see below).

2.4. Examples of Use

Figure 3 illustrates a simple example to run SMRT with a single-layer snowpack.

All the parameters describing the snowpack are first introduced: thickness, snow grain radius (or correlation length), and snow density. Surface parameters describing surface roughness are also needed to estimate the surface backscatter. If the IEM model is used, the interface is described with the surface RMS height (σh) and the correlation length of the surface (l_c). Geometrical optics is initialized with the Mean Square Slope (MSS). As seen in the previous section, the user can choose the adapted configuration considering the roughness scale. In Figure 3, the surface is considered smooth enough to use the IEM model.

The snowpack is created with the snow parameters and the created interface. Several options are proposed in SMRT to define the representation of the snow microstructure. In Figure 3, the 'exponential' one is used (see Section 2.1).

Several altimetric sensors were implemented in the altimetric version of SMRT (see Section 2.3). Here we simulate the waveform in the Ku band with the sensor parameters of the Envisat satellite.

The user can choose between several electromagnetic models. Here we use the IBA theory, meaning that the scattering and absorption coefficients and the refraction index are calculated following Matzler (1998). 'nadir_altimetry" as argument of the make_model function indicates to use the altimetric solver introduced in the previous section to solve the RT equations. Several options can be chosen: 1) if 'skip_pfs_convolution' is True, SMRT outputs the vertical scattering distribution only, and skip the convolution with the PFS, 2) if 'return_contributions' is True, the total echo is split into its three components: the total, surface, internal interface and volume contributions.

The SMRT documentation is available online (https://www.smrt-model.science/). The documentation of the nadir-altimetric solver is included in the code and will be automatically made available once integrated in the SMRT master repository.

Inputs

```
## Prepare inputs
thickness = [100.0]
density = 350.
temperature = 225.0
# snow grain size parameter
corr_length = 0.0013
# surface parameter
rough_rms = 0.005
rough_length = 0.04
```

Snowpack

```
## Create sublayers interfaces and snowpack
interface = make_interface("iem_fung92", roughness_rms=rough_rms, rough_length=long)
snowpack = make_snowpack(thickness=thickness, microstructure_model="exponential", corr_length=corr_length,
                         density=density, temperature=temperature, interface=interface)
```

Sensor config

```
## Create the sensor
sensor = envisat_ra2('Ku')
```

Choose model

```
## Create the model
m = make_model("iba", "nadir_altimetry",
               rtsolver_options=dict(skip_pfs_convolution=False, return_contributions=True))
```

Run

```
## run the model SMRT
result = m.run(sensor, snowpack)
```

Outputs

```
## Outputs:
print(result.sigma())
```

Figure 3: Example of Python code to run SMRT. The snowpack is a simple one-layer snowpack.

FORM-NT-GB-7-1

3. Intrinsic validation of the total backscatter

3.1. Comparison between the two solvers

We first checked that the energy was well conserved with the new time-dependent radiative transfer solver ('nadir-altimetric') implemented in SMRT. To do so, we compared the two total backscattering simulated with SMRT, using successively the DORT solver (i.e time independent) and the nadir-altimetric solver. The time dependence introduced in the nadir-altimetric solver mainly impacts the volume backscattering. Hence, to compare the two solvers, we used a snowpack with transparent interfaces to simulate the volume contribution only. Total backscattering are simulated using a snowpack with a single layer, described with a snow temperature of 220 K, a snow density of 250 kg m-3, a thickness of 1000 m, and a radius of 0.9 mm for case 1 ('large grains') and of 0.2 mm for case 2 ('small grains'). Surface roughness is neglected here since DORT does not account for the bi-directional reflectance yet.

The DORT solver has been used by the SMRT community for three years and has been well validated, it is our reference here. DORT computes the total backscattering at given incidence angles, a given frequency and in vertical/horizontal polarizations, considering multiple scattering (of any order, but without the possibility to split the successive orders). To retrieve the total backscattering with the nadir-altimetric solver, the altimetric backscatter is normalized by the radar signal simulated using the calibration sphere (see previous Section 2.3.3). We estimate a total backscattering coefficient at nadir for a given frequency.

Figure 4 shows the total backscattering simulated in the Ku band as a function of the incidence angle, using a snowpack with small snow grains (case 2). There is a good agreement between the two solvers at nadir, with similar total backscattering coefficient values, showing the energy is well handled by the nadir-altimetric solver.

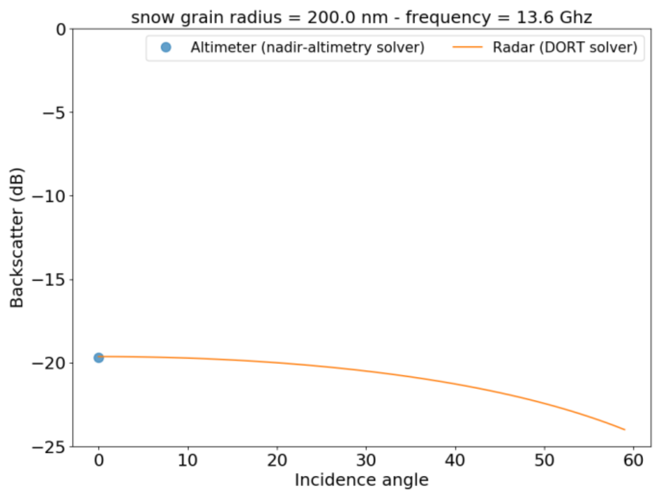

Figure 4: Total backscattering (in dB) as a function of the incidence angle at 13.6 GHz. SMRT simulations are performed with small snow grain size (0.2 mm).

Figure 5 shows the total backscattering simulated at nadir as a function of the frequency, using a snowpack with small snow grains or large snow grains. Both solvers give different total backscattering at high frequencies and this difference is larger for snowpack with larger snow grains. This result comes from the fact that the DORT solver accounts for multiple scattering, whereas nadir-altimetric is limited to single scattering (first order solution of the radiative transfer equation using the iterative method). At high frequencies and/or for snowpack with large snow grains, the difference of total backscatters between the two solvers is significant (Fig. 5) and the contribution of the second and higher orders of scattering on the radar signal should be considered for altimetric simulations. However, it involves much more complex calculations of the time delay which is not a solved problem yet (to our knowledge). Indeed, the first order of scattering involves simple path for which it is easy to determine the time travel from the satellite to the echo and back. In contrast, for multiple scattering (higher-order contributions), the paths are multiple owing to the integral over the angles in the scattering term of the radiative transfer equation. Each path has a different length, so a different delay and this is a priori not linear (i.e. not a simple convolution). The integral would need to be calculated numerically. An alternative is to use a Monte Carlo method known, mathematically, to be suitable for complex integrations, and physically, which has a nice interpretation (photon path here). An avenue is to implement Monte Carlo technique for the second and higher orders only, on top of the nadir_altimetry module which efficiently and accurately computes the first order.

Hence, the nadir-altimetric solver is reasonably accurate at low frequency and/or for weakly scattering media. In any case, second and higher orders would add more backscatter (not less) and this signal would arrive later than the first order signal. So the expected impact is a higher and smoother leading front, and longer edge, as much as frequency and grain size are increasing.

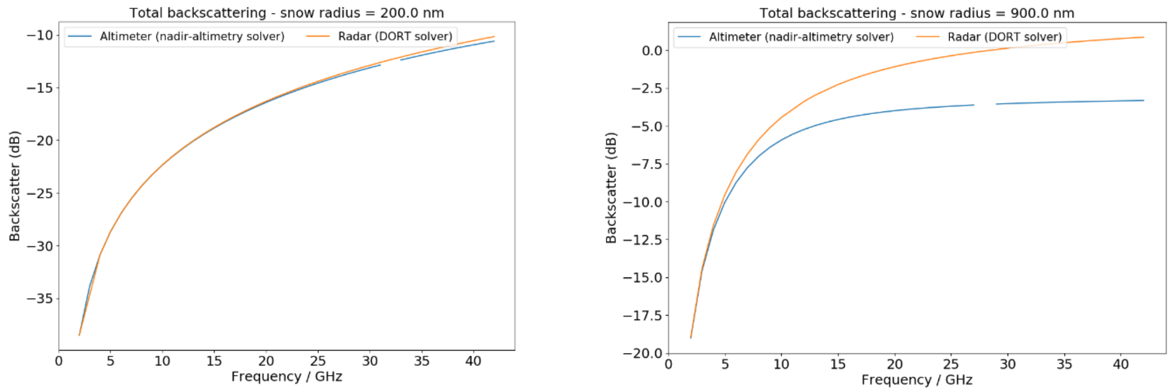

Figure 5: Total backscattering simulations as a function of frequency using a snowpack with small snow grains (left) and large snow grains (right).

3.2. Interaction orders between electromagnetic wave and snow

To investigate the validity range of the 1sr order, several SMRT simulations are performed with DORT and nadir_altimetry by varying snow grain radius and frequency. The difference between the two simulated total backscatters is calculated and we consider that differences below 1 dB are acceptable.

Figure 6 shows the domain of validity as a function of snow grain size and frequency. Multiple scattering is negligible when the snow grains are smaller than 0.8 mm, 0.5 mm and 0.2 mm, at 3.2 GHz (S band of Envisat), 13.6 GHz (Ku band of Envisat2), and 36 GHz (Ka Band), respectively. For comparison, the range of variations of the snow grain radius previously observed in Antarctica is of 0.1 to 1 mm (Surdyk and Fily, 1993).

FORM-NT-GB-7-1

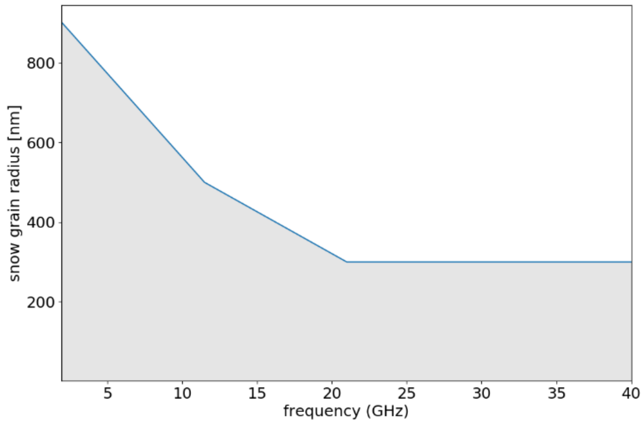

Figure 6: Domain of validity (in grey) for SMRT simulations using the nadir-altimetric solver. The gray area is the area where SMRT simulations with Dort and nadir_altimetry, using the same initial configuration, are less than 1 dB different.

4. Comparison to Lacroix et al. 2008 's model

The model developed by Lacroix et al. (2008) is similar to the new altimetric version of SMRT, except that the snow microstructure is represented as an ensemble of independent spheres. Although SMRT is able to represent snow microstructure in a more realistic way, the 'independent sphere' configuration is also available. Here, SMRT is evaluated by comparing simulations with those of the Lacroix et al. 2008's model (called 'Lacroix08'), using the same inputs and configurations.

To model the vertical distributions of snow parameters, the density profile is described with a polynomial equation of order 4, using constant coefficients retrieved from in situ observations of density profiles at Talos Dome:

$$p(z) = p(z=0) + a.z + b.z^2 + c.z^3 + d.z^4 \quad [8],$$

with a = 0.0140178, b = -0.00013531, c = 5.8617e-7, and d = -9.3228e-10. The surface density is an input of the model. The complex relative dielectric constant of snow is calculated using the formulation of Tiuri et al (1984), and depends on snow density and snow temperature. The temperature and the snow grain size are constant over the entire profile. The snow surface roughness is represented by the surface rms height of roughness features (σr), and the correlation length of roughness features (lc). Table 1 summarizes the model inputs, in relation to the SMRT inputs.

Inputs	density (kg m-3)	snow grain radius (mm)	surface rms height (mm)	correlation length (mm)	snow temperature (K)
Lacroix	var.	cst	cst	cst	cst
SMRT	var.	var.	cst	cst	var.

Table 1: List of snow parameters given as input of the model. Snow parameters considered as constant over the depth profile are noted 'cst', and parameters represented as variable, i.e. one value per snow layer, are noted 'var.'.

4.1. Comparison

- <u>SMRT configuration</u>

In this subsection, we present the SMRT configuration for the comparison with the Lacroix et al. 2008's model (Lacroix08).

As seen in the previous section, the surface/interface scattering properties have to be estimated using the IEM method developed by Fung (1992). In this project, this surface scattering model has been implemented in SMRT with the new 'iem_fung92' module. In terms of coding, the surface/interface is initialized as follows:

```
> interface = make_interface("iem_fung92", roughness_rms=sigma_r,
                              corr_length=lc)
```

In SMRT, the existing 'ice_permittivity_tiuri84' module allows to calculate the permittivity as a function of the snow density following Tiuri et al. (1984), as in Lacroix08. Furthermore, among several existing representations for the snow microstructure, the 'independent_sphere' module is available to follow the same representation as in the Lacroix08. The snowpack is thus built as follows in SMRT:

```
> snowpack = make_snowpack(thickness=layer_thickness,
                           microstructure_model="independent_sphere",
                           radius=radius, density=density,
                           temperature=temperature, interface=interface,
                           ice_permittivity_model=ice_permittivity_tiuri84)
```

The electromagnetic model used in Lacroix et al. (2008) applies the Original Improved Born Approximation theory, meaning that the absorption is calculated with the original formula in Matzler (1998). The 'IBA_original_Tiuri' electromagnetic model class was added to SMRT (and used only for this comparison), and is used to initialize the electromagnetic model as follows:

```
> emmodel = make_model(IBA_original_Tiuri, "nadir_altimetry",
                       rtsolver_options=dict(skip_pfs_convolution=False,
                       return_contributions=True, theta_inc_sampling=32))
```

The options of the 'nadir_altimetry' RT solver were described in Section 2.4.

Lacroix et al. (2008) compare the dual frequency ENVISAT signal with their altimetric model, i.e. for both S and Ku bands. We make sure to use the same sensor configuration in SMRT and in Lacroix08. The sensor parameters are details in Table 2.

Parameter	S band	Ku band
Center frequency	3.2 Ghz	13.6 GHz
Bandwidth	160 MHz	320 MHz
Antenna beamwidth at 3 dB	5.5°	1.35°
number of gate	128	128
nominal gate	20	45

Table 2: ENVISAT altimetric radar characteristics (from Lacroix et al., 2008).

- <u>Evaluation of scattering coefficients</u>

The quality of the new SMRT modules is first analysed with a single-layer snowpack composed of large snow grains (radius of 0.6 mm, i.e. high volume contribution). The density is of 340 kg m^{-3}, the mean temperature is equal to 225 K, and the surface roughness parameters σr and lc are equal to 3 mm and 4 cm, respectively. These latter values respect the validity domain of IEM (see previous Section).

Figure 7 shows the surface backscattering variations as a function of the surface rms height parameter σr, in the Ku and S Bands. SMRT simulations are similar to Lacroix08 simulations, with a RMSE of 0.01 and 0.02 in Ku and S Bands, respectively. This result shows that the IEM model implemented in SMRT is correct.

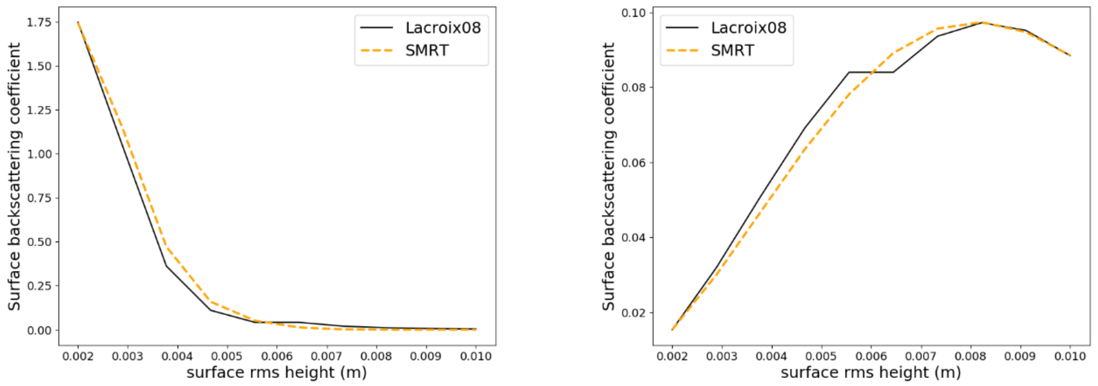

Figure 7: Variations of the nadir surface backscattering coefficient using the IEM method (Fung 1994) as a function of the surface RMS height in Ku band (left) and S Band (right). Simulations are performed with the Lacroix et al. 2008's model (Lacroix08, dotted orange line) and the SMRT model (SMRT, black line).

Figure 8 shows scattering coefficient values ('ks') as a function of the snow grain radius, in the Ku and S bands. SMRT and Lacroix08 simulations are in agreement in the S band. The volume contribution is low in the S Band because of weak scattering by snow grains. In the Ku Band, the difference between SMRT and Lacroix08 simulations increases when snow grains become larger. In Lacroix08, the scattering coefficient is estimated using the Eq. 32 of Matlzer (1998), which makes the approximation of small angles to simplify sinus terms, while in SMRT the scattering coefficient is calculated numerically by integration over the scattering angle. This difference of formulations explains the difference of ks observed in Fig 8.

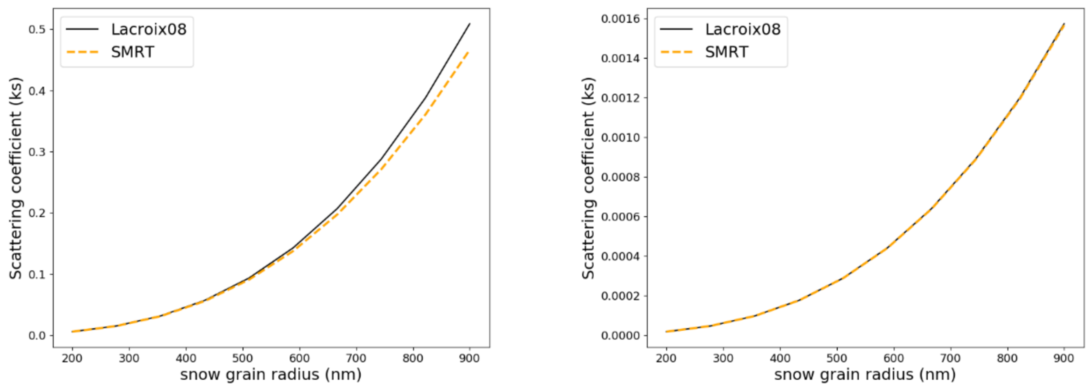

Figure 8: Variation of the scattering coefficient as a function of the snow grain radius in Ku Band (left) and S Band (right). Simulations are performed with the Lacroix et al. 2008's model (Lacroix08, dotted orange line) and the SMRT model (SMRT, black line).

➢ Altimetric waveforms

With a single-layer snowpack : large / small snow grains

Figure 8 shows the waveforms simulated with SMRT and Lacroix08 using two different snowpacks: one with large grains (i.e high volume contribution) and one with small snow grains (i.e. high surface contribution). Results in the Ku band show perfect agreement between the two models.

These two snowpacks are used to assess the sensitivity of the waveform shape to snow parameters. Surface echo mostly depends on snow roughness and snow density values, while the volume echo (penetration of the signal within the snowpack) depends on the dielectric losses, i.e. absorption and scattering, which mainly vary with snow grain sizes and internal stratification reflection (Rémy et al., 2012). The latter contribution also strongly depends on the frequency.

Fig. 9b and 9d show that a snowpack with small snow grains has a negligible volume echo, while Fig. 9a and 9c show that the signal penetrates deeper within a snowpack with large snow grains (higher volume echo). The presence of a snowpack with large snow grains can have important consequences on retracking algorithm outputs. Indeed, the volume echo introduces a 'delay' on the echo amplitude. This can lead to very different values of the leading edge width, according to the structure of the snow media.

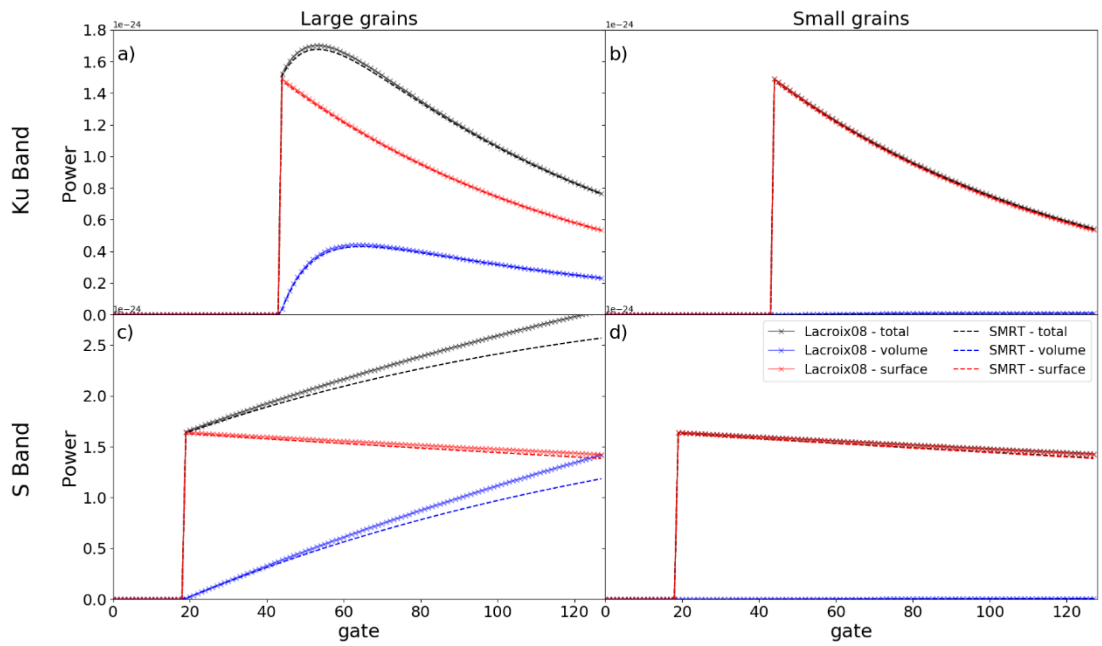

Figure 9: Waveforms simulated with SMRT (dotted lines) and the Lacroix08 (cross) with a) Ku band and large snow grains, b) Ku band and small snow grains, c) S band and large snow grains, d) S band and small snow grains. The total waveform (black) is the sum of the surface echo (red) and the volume echo (blue).

With a multi-layer snowpack over the Antarctic ice sheet (Vostok)

For the evaluation of the simulated altimetric waveform, we use a synthetic snowpack described in Lacroix et al. (2008). This synthetic snowpack is built to be representative of the Vostok Lake site (lat=104.12°, long=-76.57°). This site was chosen because it has virtually no slope. The snow parameters were retrieved by fitting the waveform simulated with Lacroix08 to the real waveform observed with Envisat-2 in the S and Ku Bands. To do so, the range of variations of the snow parameters were bounded based on in situ observations (see Lacroix et al., 2008 for details on the inversion). The annual mean temperature is 220 K. Table 3 details the snow parameters of the Vostok synthetic snowpack. The density profile is estimated using eq. [3] (Figure 9).

	surface density (kg m-3)	snow grain size (mm)	surface rms height (mm)	correlation length (mm)	Temperature (K)
Lake Vostok	240.0	0.9	3.9	140.0	220.0

Table 3: Snow parameters at Lake Vostok as described in Lacroix et al. (2008).

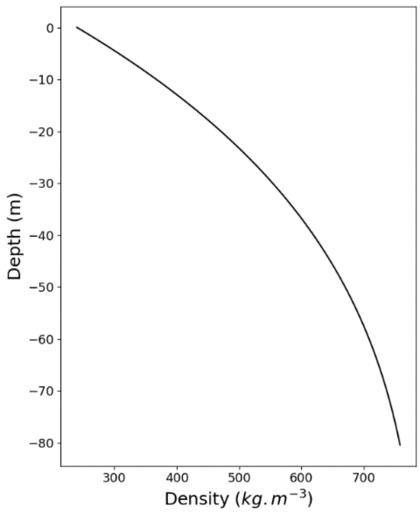

Figure 10: Density profile of the synthetic snowpack representing the Lake Vostok site.

Using this synthetic snowpack as input, altimetric waveforms are simulated with SMRT and Lacroix08. Results are shown in Figure 10. Statistical performances of SMRT are shown in Table 4 by considering Lacroix08 as the 'True' observation. The SMRT simulations agrees with Lacroix08 simulations, with a RMSE of 1.7 % and 1.4 % in the Ku and S bands, respectively.

The Vostok synthetic snowpack has large grains in comparison to previous in situ observations (see Table 2 in Lacroix et al., 2008). As explained in previous sections, large snow grains cause high volume echo. This is why, at the Ku band (Fig. 10a), the shape of the waveform is rounded compared to the waveform shape commonly observed over oceanic surfaces (surface echo only). This rounded shape is close to the waveform observed over the Antarctic ice sheet.

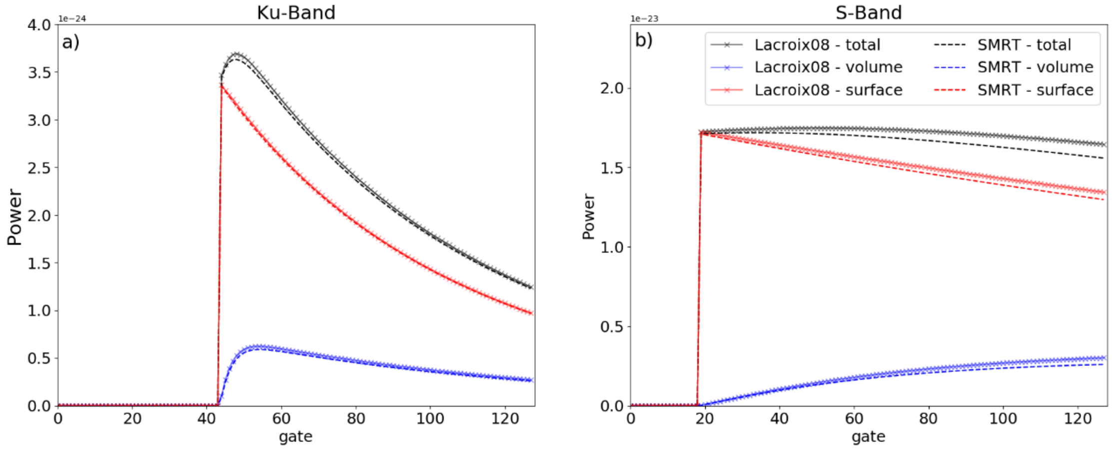

Figure 11: Waveform simulated over Lake Vostok with SMRT (dotted lines) and the Lacroix et al 2008's model (cross) in the a) Ku band , and b) S-Band.

Band	Normalised RMSE [in %]			Bias		
	Total	Volume	Surface	Total	Volume	Surface
Ku (13.6 Ghz)	1.7	1.1	0.7	-1.9e-26	-1.3e-26	-0.7e-26
S (3.2 GHz)	1.4	1.5	2.1	-1.3e-25	-1.8e-25	-2.7e-25

Table 4: Statistical performances of waveform simulated with SMRT compared to the Lacroix et al. 2008's model.

- <u>SMRT adaptation for the comparison with Lacroix08.</u>

In Lacroix08, the volume backscatter (i.e the bistatic scattering coefficient in the backward direction) is assumed equal to the scattering coefficient ks, and ks is used to build the volume vertical backscattering distribution. This is a rough approximation (or a mistake). In SMRT, ks is used to estimate the extinction coefficient ke, but the bistatic scattering coefficient (i.e. phase matrix) in the backward direction is used to calculate the volume vertical backscattering coefficient. Under IBA and for small grains, the bistatic scattering coefficient is related to 1.5 x ks. Thus, for the comparison with Lacroix08 only, and despite the rough approximation/possible mistake, we have added a factor /1.5 to the simulated volume backscatter in SMRT, in order to use the same formulation as in Lacroix08.

To be coherent with Lacroix08, the SMRT PFS is estimated with the classical radar equation integrated over the illuminated area (see Eq. 3 in Lacroix et al., 2008). In this project, several PFS were implemented in the nadir_altimetry module, and validated with the numerical PFS, such as: the PFS introduced by Brown (1977) for a perfect nadir case, and the PFS proposed by Newkrik and Brown (1992). Compared to the classical Brown (1977), this latter PFS takes into account the asymmetry of the antenna pattern in the co and cross-track direction. Both PFS account for the Earth's curvature.

The pulse of the radar is here a perfect dirac (no pulse width effect is considered here). However, for further studies, the Point Target Response (PTR) has been implemented in the SMRT 'nadir-altimetry' module to model the pulse with a gaussian. The width of the pulse is an input parameter.

4.2. A realistic synthetic snowpack

The main difficulty in the validation of an altimetric waveform model is due to the lack of in situ data on snow properties over sea ice and ice sheets. The question of how to use in-situ measurements or outputs from thermodynamic models as inputs of such altimetric waveform model is a general and difficult issue. We have made some progress using in-situ data collected on a 1300 km traverse in Antarctica, with very contrasted surface roughness and snow. However, this activity is beyond the scope (and the timeframe) of the 1-year PMM. Here, we propose to create and investigate two study cases representing the large ice-sheet with a tick dry and cold snowpack. The first synthetic snowpack is a multi-layered synthetic snowpack, and the second has a single layer and is used for the sensitivity analysis presented in the next Section.

4.2.1. Method

The Vostok synthetic snowpack was obtained by fitting the Lacroix08 simulated waveforms to Envisat observations (in the S and Ku Bands). Hence, the Lacroix08 simulated waveforms can be considered close to observations, and are further considered as the 'true' observations. Nevertheless, snow parameters of the Vostok snowpack were retrieved by representing the snow microstructure as a collection of independent spheres and using Tuiri equation for the permittivity, which are unrealistic. To build the new snowpack, the snow parameters have to be adjusted using an adapted representation of the snow microstructure, and Matzler's permittivity. Moreover, the Lacroix08 model uses the original IBA formulation. An updated version of the IBA theory has been proposed by Matlzer, and is the default in SMRT. We thus use the recent IBA version in the next SMRT simulations.

More complex representations were developed in the past to model snow as a dense medium. For instance, the practical implementation of IBA in the MEMLS snow model used the exponential autocorrelation function to represent snow microstructure, and it has been widely validated by the passive microwave community. We keep the same inputs as in Section 4.2 for SMRT simulations, except that the snowpack is initialized with the 'exponential' module to describe the snow microstructure, such as:

```
> snowpack_expo = make_snowpack(thickness=th,

                                microstructure_model="exponential",
                                corr_length=l_corr,density=density,
                                temperature=temperature,interface=interface)
```

Figure 12 shows the altimetric waveforms modeled by changing the snow microstructure representation from 'independent sphere' to 'exponential' in SMRT, and the recent IBA version. The difference is particularly high in the Envisat S band, with normalised RMSEs of 5.1 % and 102.1 % in the Envisat Ku and S bands, respectively (see Table 5 for statistics).

The configuration changes impact both the volume and surface contributions. Thus, to adjust the waveform simulated with SMRT, and considering the 'exponential' model, to the 'true' observation, we fit the snow grain radius and the surface snow density. To do so, the optimisation is performed using a differential evolution method developed by Storm and Price (1997) over the two waveforms simulated in the Ku and S bands.

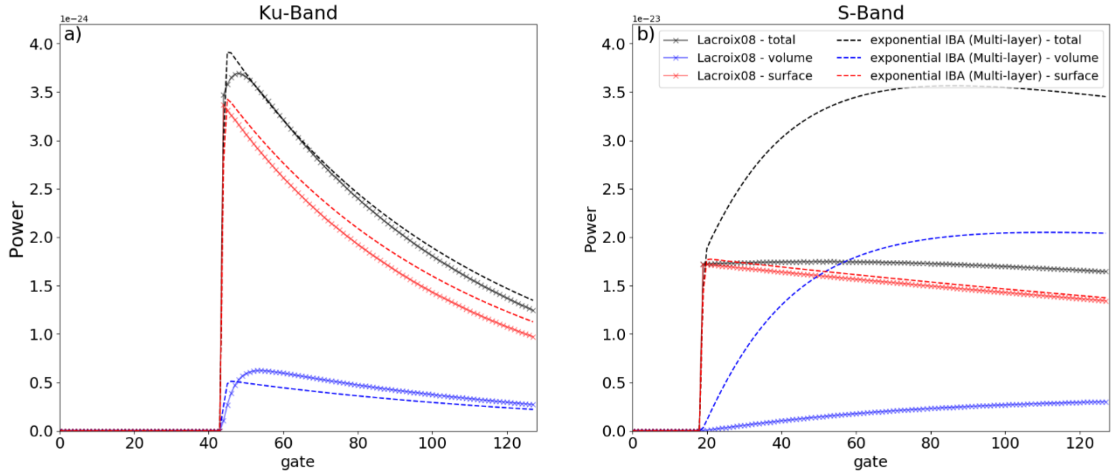

Figure 12: Waveform modeled with Lacroix08 (cross) and SMRT (dotted lines) using the Vostok synthetic snowpack in the Envisat Ku Band (right) and S band (left). SMRT is run with an exponential representation of the snow microstructure (dotted lines) and a snow grain radius of 0.9 mm. The total echo is in black, the volume echo in blue and the surface echo in red.

Snowpack	Band	Normalised RMSE (in %)			Bias		
		Total	Volume	Surface	Total	Volume	Surface
Multi-layer	Ku	5.1	30.3	11.0	4.0e-26	-5.8e-26	9.7e-26
	S	102.1	864.8	3.7	132.2e-25	125.9e-25	339.6e-25

Table 5: Statistical performances of waveforms simulated with SMRT when the snow microstructure is modeled with the 'exponential' module. The Lacroix et al. 2008's simulations are the 'true' synthetic observations.

4.2.2. Synthetic snowpack

<u># Case 1: multi-layered snowpack</u>

The retrieved snow grain radius is equal to 0.365 mm and the adjusted surface density is equal to 235 kg m-3. Figure 12 shows the fitted SMRT waveforms compared to the Lacroix08's waveforms. Waveforms are in agreement, and the normalized RMSEs are equal to 5 % and 4% in the Ku and S bands, respectively (see Table 6 for statistics). It mainly impacts simulations in lower frequencies (S band). A snow grain radius of 0.365 mm is coherent with previous in situ observations (see Table 2 of Lacroix et al., 2008).

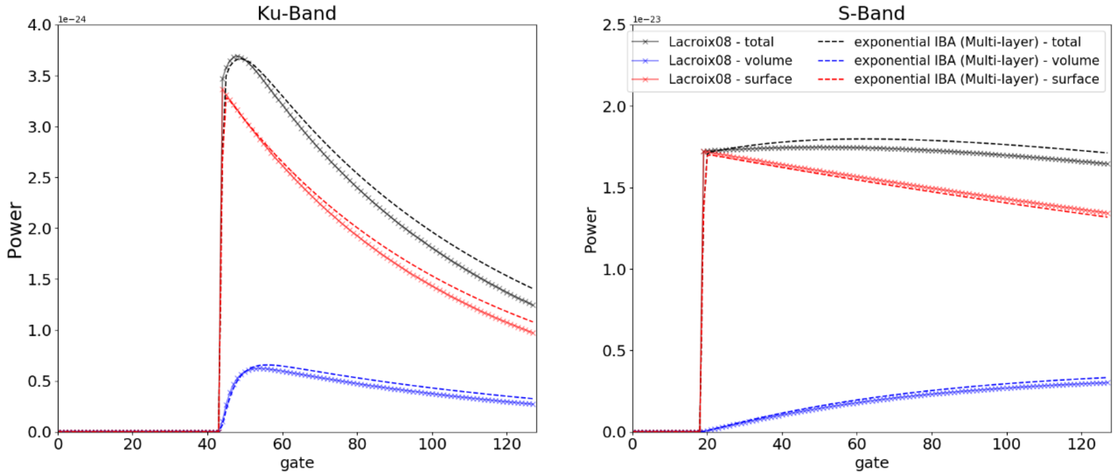

Figure 13:SMRT waveforms (dotted lines) fitted to the true synthetic observations (Lacroix08, cross) in the Envisat Ku Band (right) and S band (left). SMRT is run with an exponential representation of the snow microstructure (dotted lines) and a snow grain radius of 0.387 mm. The total echo is in black, the volume echo in blue and the surface echo in red.

Snowpack	Band	Normalized RMSE [in %]			Bias		
		Total	Volume	Surface	Total	Volume	Surface
Multi-layer	Ku (13.6 Ghz)	5.0	14.7	7.2	7.3e-26	3.0e-26	4.2e-26
	S (3.2 GHz)	4.0	11.7	2.9	3.9e-25	1.6e-25	-2.1e-25
single-layer	Ku (13.6 Ghz)	8.6	17.8	7.2	8.0e-26	3.8e-26	4.2e-26
	S (3.2 GHz)	6.4	32.1	2.9	5.8e-25	7.8e-25	-2.1e-25

Table 6: Statistical performances of waveforms simulated with SMRT model when the snow microstructure is modeled with the 'exponential' module. Snow parameters are optimized by fitting SMRT to Lacroix08 simulations. 'MEANobs' is the mean of the true synthetic observation. Normalized RMSE is estimated as: RMSE/MEANobs.

<u># Case 2: single-layered snowpack</u>

To build a single-layer synthetic snowpack, the same snow parameters as those of the Vostok snowpack are taken, except that SMRT is run with a constant density. The waveform is adjusted to Lacroix08's waveform by fitting both the mean density and the snow grain radius. The best fit is obtained with a mean density of 235 kg m-3, and a snow grain radius of 0.375 mm. Fig. 14 show SMRT simulations with the optimized single-layer synthetic snowpack. A mean density of 235 kg m-3 over the entire profile is not realistic. The model fits the Lacroix08s' waveform very well, with normalized RMSEs equal to 9% and 6% in Ku and S bands, respectively (Table 6). In the Ku band, the radar waves penetrate no deeper than 10 m, but in the S band the signal penetrates much deeper than 1000 m.

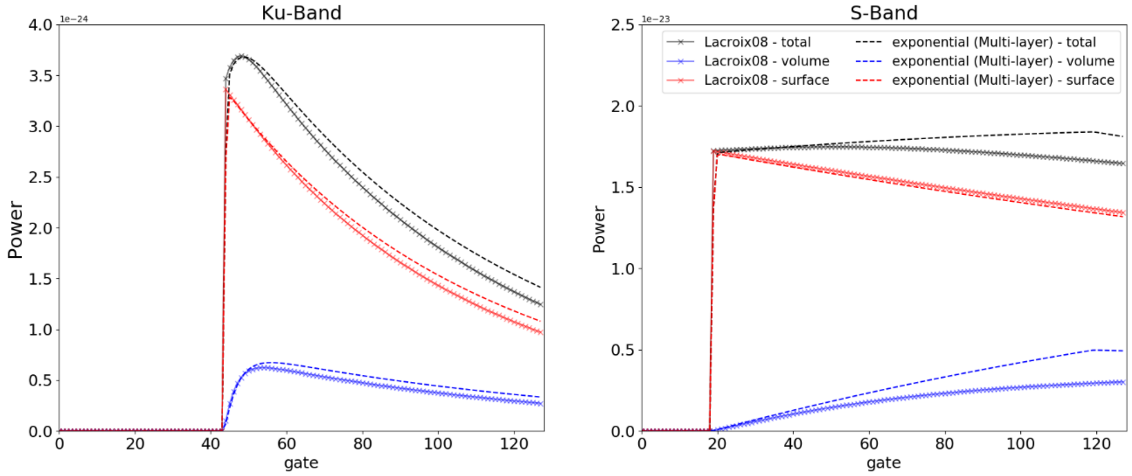

Figure 14: Same as Figure 12 but with a single layer snowpack.

The snow parameters of both optimized snowpacks (multi layer and single layer) are summarized in Table 7.

	density (kg m-3)	snow grain radius (mm)	surface rms height (mm)	corr. length (mm)	T (K)	layer thickness (m)	σtot (dB)
multi-layer snowpack	235-757	0.365	4	140	220	0.1	3.7
single-layer snowpack	235	0.375	4	140	220	80	3.7

Table 7: Synthetic snowpack derived for Vostok from Lacroix et al. 2008. For the multi-layer snowpack, only the density varies with the depth (with Eq. 3). The snow depth is 80 m.

5. Sensitivity study

The single-layer snowpack is used to analyse the impact of snow parameter variations on the waveform shape in the Ku and Ka bands.

We first analyse the sensitivity of the volume contributions by varying the snow grain radius and the mean density. Second, the roughness sensitivity is studied to investigate the impact on the surface contributions.

5.1. Sensitivity to the volume contributions

Waveforms are simulated with SMRT using the exponential microstructure, and the G0 model. Snow properties are taken from the optimized single layered snowpack presented in Table 7, and we used a mean square slope (mss) fixed to 0.01 (rough estimate, similar to what is used in the literature for oceanic surfaces). Simulations are run by varying the snow grain radius from 0.1 to 0.4 mm, and then by varying the mean density from 235 kg m-3 to 350 kg m-3. Table 8 summarizes the range of variations of these inputs. We compare the sensitivity of the dual-frequency signal in the Ku and Ka bands. Results are shown in Figure 14 and summarized in Table 9. The relative variations is estimated with the following equation: 100.(noised_simulation - original_simulation) / original_simulation.

Snow parameter	units	Min value	Max value
Density	kg m-3	235	350
Snow grain radius	mm	0.1	0.4
surface mss height	no units	0.008	0.012

***Table 8**: Range of variation of snow parameters in our sensitivity analysis.*

In the Ku band, both the snow density and snow grain size variations strongly affect the waveform, by about 40 % (Fig. 15a). A density variation mainly influences the amplitude of the surface contribution, while the snow grain size mainly affects the volume contribution. The latter parameter greatly affects the shape of the waveform, mainly the leading edge width. This waveform parameter is commonly retrieved by retracking algorithms and used to get information on the local topography and the wave penetration depth. A distortion of this waveform parameter can induce an altitude bias (Legrésy et al., 2005).

In the Ka band, the radar echo mainly comes from the volume scattering (Fig. 15c and 15d). It is worth noting that this is counter-intuitive as several studies of the altimetric observations indicate that the Ka band is dominated by surface echo. To reconcile both, it is worth mentioning that the volume echo predicted by the model is coming from the near-surface, and could therefore be wrongly interpreted as a “surface” signal, especially compared to the Ku and S bands where the volume echo is coming from deeper. The waveform is highly sensitive to the snow density (variation >50% with a density from 235 kg m-3 to 350 kg m-3, see Table 9), but a density variation weakly affects the leading edge width. On the contrary, as in the Ku band, a snow grain size variation strongly changes the shape of the waveform (Fig 15d).

In this sensitivity study, the simulations are conducted in the Ka band although the snow grain radius is higher than 0.2 mm, outside the validity domain of the 1st order approximation (see Section 3.2). Nevertheless, even if negatively biased by neglecting the higher order, this analysis gives important information about the behavior of the waveform at common frequencies.

Parameter variations	Ku Band			Ka Band		
	radius	density	mss	radius	density	mss
Min value	- 44.7 %	0 %	-7.1 %	18.0 %	0 %	-8.9 %
Max value	-0.2 %	40.7 %	10.7 %	-2.4 %	52.9 %	13.3 %

Table 9: Percentage of waveform variations by varying each snow parameter of ± 20%.

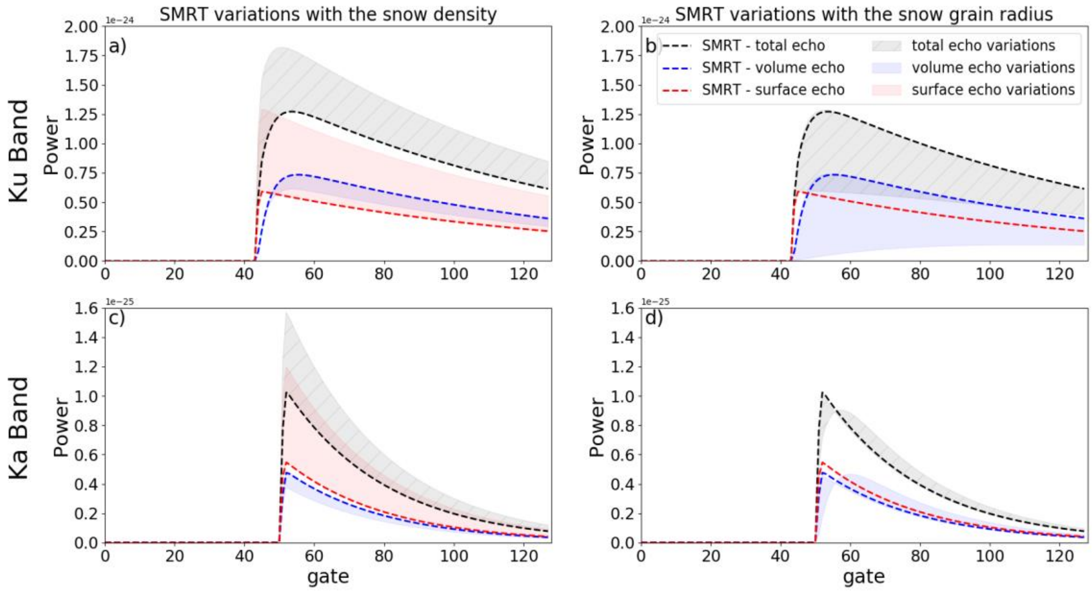

Figure 15: Waveforms simulated with SMRT (exponential microstructure) with the single snowpack and where a) the snow density varies from 193 to 290 kg m-3 in the Ku band, b) the snow grain radius varies from 0.310 to 0.464 mm in the Ku band, c) the snow density varies from 193 to 290 kg m-3 in Ka band, d) the snow grain radius varies from 0.310 to 0.464 mm in Ka band.

5.2. Sensitivity to small scales roughness

SMRT simulations are performed by varying the surface mss by ± 20%. Results are detailed in Table 9 and shown in Figure 16, in the Ku and Ka bands.

In the Ku band, the amplitude of the surface echo varies by about ± 8.9 % when the surface mss changes by ± 20% (from 0.008 mm to 0.012 mm, see Table 8). It is strong, especially knowing that this surface parameter is also notoriously difficult to measure in the field, and variable over the ice-sheet. A small error on the mss parameter can thus induce a strong bias on the total backscattering coefficient. Note that the mss variations only affect the backscattering coefficient, by changing the amplitude of the waveform, and the sensitivity to the leading edge width and to the trailing edge slope is low.

In the Ka band, the mss parameter changes the amplitude of the total echo by ± 11.1% by varying of ± 20%. Logically, it mainly impacts the surface echo, but the volume echo is weakly affected too. It is due to the fact that the mss changes the transmission contribution, which impacts on the simulated volume echo.

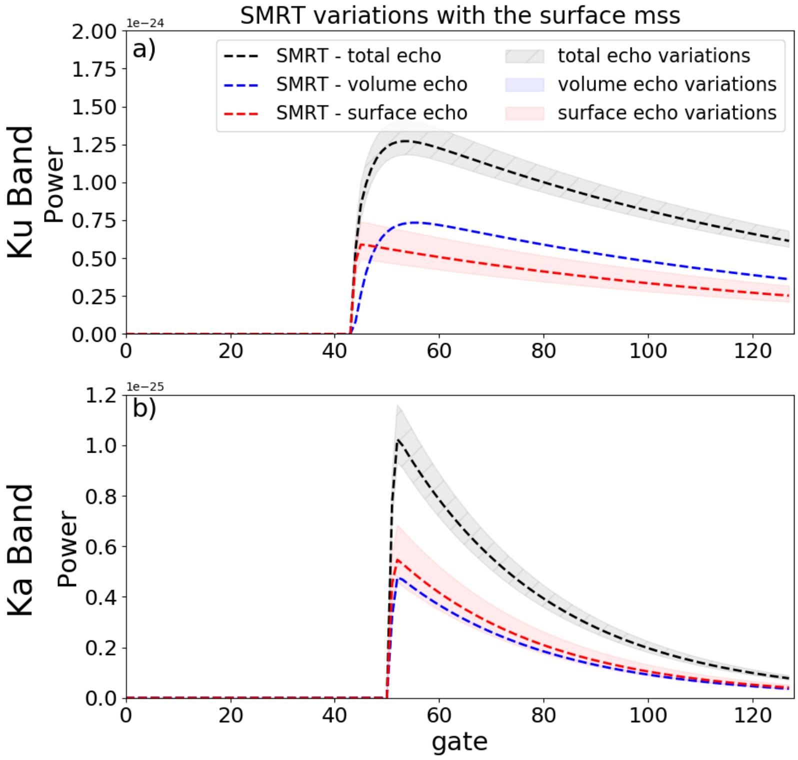

Figure 16: Same as Figure 14 but with surface roughness parameters variations.

6. SMRT / AltiDop combination

6.1. AltiDop presentation

Since the inception of radar altimetry, 25 years ago, CLS developed and continuously improved several numerical simulation tools to understand and study the altimetry measure. In this study, we use “AltiDop”, a versatile simulator, with an end-to-end capability: from scene generation to level-2 retracking. It has the capability to simulate altimetry waveforms in multiple ways:

- The waveforms are simulated through a numerical pixelized-scene. Each pixel representing a facet, a portion of the scene, for which the altimetry signal backscattered is computed using the radar equation (see equation 8). The signal therefore depends on:
  - Antenna/facet distance
  - Antenna gain pattern
  - Facet radiometric model, which describes the interaction between signal and facet, in particular the backscattering variation as function of the incident angle
  - Mean square slope (itself depending on sea state over ocean)
  - Facet slope

  The simulator is mainly used for oceanic studies, and it is possible to generate scenes with facets elevations and slopes reproducing realistic sea states: windsea and swell conditions notably.

- In recent years, some developments have been made to generate scenes modeling simple inland waters scenarii. In these cases, the radiometric model can change from one pixel to another to reproduce the surface heterogeneities.
- It is possible to add topographic surface slopes to the scene. Moreover, first tests have been made to integrate topography directly coming from the Reference Model Of Antarctica (REMA), a high resolution (8 meters) Digital Elevation Model (see section 7.7.4)
- It is possible to directly simulate model waveforms, in power (I & Q), to avoid any speckle noise. Model waveforms can be simulated in LRM/SAR/LR-RMC modes. Alternatively, it is possible to simulate complex radar pulses (I2+Q2) at Pulse Rate Frequency and run dedicated level-1 processing to build LRM/SAR/LR-RMC waveforms similarly as it done by ground segments algorithms.

  ⇨ ***In this study we simulate only power model waveforms to precisely assess the waveform shapes, without any speckle noise addition***

- Waveforms can be simulated along simple orbit cases (constant altitude or constant radial speed, but it is also possible to use real orbital data.
- Simulations are possible with all the current and past altimetry missions. The simulator takes into account their specific properties (altimeter instrument, antenna, orbit…) listed in a configuration file. For this study the CRISTAL mission and its altimeter have been added to the list of sensors.

There are three major operating stages during an AltiDop simulation:

1) **Scene generation**

A numerical scene is generated, corresponding to a 2D data matrix, with each matrix element representing a surface facet. Facets elevation can be computed in several ways:

- A basic scenario with a complete flat scene, all facet elevations are set to 0.
- A Gaussian distribution with an amplitude controlled by a Significant Wave Height defined in the configuration file
- An "oceanic wind-sea" scenario with facet elevations derived from a Pierson-Moskovitz spectrum
- An "oceanic swell" scenario with facets elevations derived from a Durden-Vesecky spectrum
- An "oceanic well + wind-sea" scenario with facet elevations derived from an Elfouhaily spectrum
- Elevations can also be set manually, by directly modifying the matrix of elevations
- Developments are ongoing to directly use the Reference Model Of Antarctica, a Digital Elevation Model of Antarctica, at 8 meters spatial resolution.

The following figures show two examples of oceanic scenes generated by AltiDop, with a wind-sea simulation (left), and a swell simulation (right):

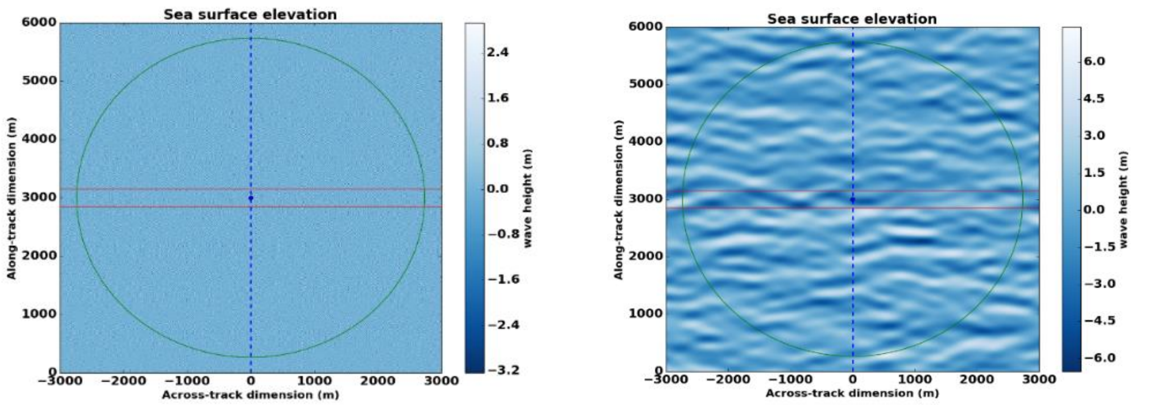

Figure 17: *Illustrations of two oceanic scenes simulated by AltiDop. A wind-sea scenario (left) and a swell scenario (right).*

2) **Radar equation computation**

The altimetry signal backscattered by each facet is computed using the radar equation, formulated by Brown [1977]:

$$\Pr = Pe\,\frac{\lambda_0^2}{(4\pi)^3}\int_{sea\ facets}\frac{G^2\sigma_0}{R^4}\,dS \qquad [8]$$

Where :

Pe : Emitted power of the antenna

λ_0 : Wavelength = c / Fc (*with c the light speed and Fc the Ka band frequency)*

R : The satellite – ground distance

G : The antenna gain
$\boldsymbol{\sigma_0}$: Backscatter coefficient
dS : Surface of a sea facet

3) Altimetry waveform construction

The altimeter range is computed for every facet given the antenna/facet distance. Thanks to this range distance the contribution of each facet is added at the correct altimeter waveform sample (or range gate). Waveforms can also be oversampled in the range dimension, allowing a numerical convolution with a realistic Pulse Target Response (PTR) with a sinus cardinal shape. The oversampling factor is set by the user.

The Figure 18 illustrates the final step of the AltiDop simulation, when the LRM power waveform (or the complex pulses) are constructed:

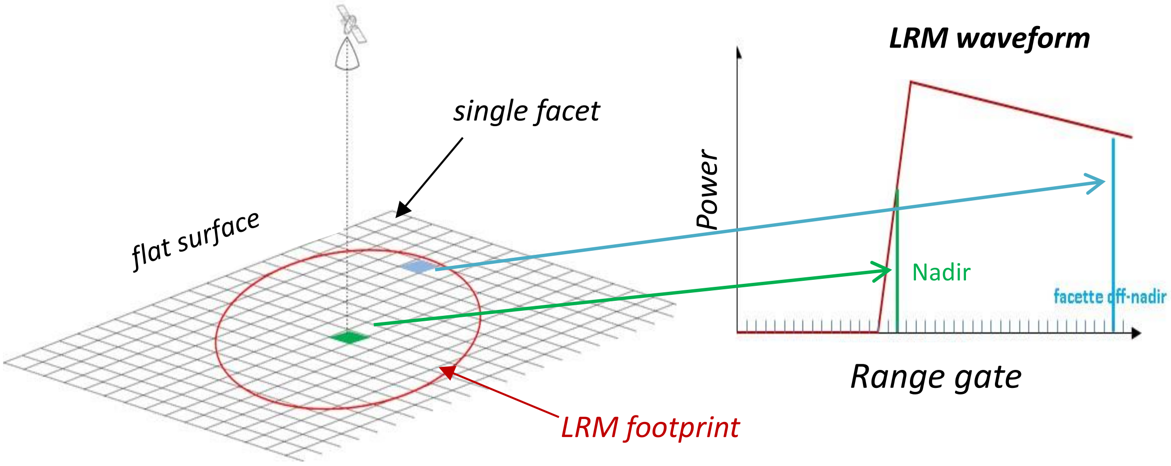

Figure 18: Illustration of the waveform construction, final step of the AltiDop simulation processing

The AltiDop simulator has been extensively used for generating LRM/SAR data over different sea scenarii, making it a highly versatile and useful tool for investigating sea state effects on low- and high-resolution mode altimetry data. Oceanic simulations have been fully validated. Biases with the CNES simulator used in Sentinel-3A Processing Prototype level-2 [Boy et al., 2017] are extremely small (less than 1cm in range and SWH). First simulations made using high-resolution REMA topography show very good agreement with real acquisitions (see section 7.7.4).

6.2. Combination of AltiDop and SMRT

6.2.1. Methodology

As already described in section 2.2, the altimetry waveform measured over snow surface can be discriminated in two components:

- **PFS** (Power From Surface): the signal backscattered at snow/air interface
- **PFV**(Power From Volume): the signal backscattered by the snowpack, with two different origins:
  - The scattering from snow grains within the snowpack (P_{grain})
  - The backscattering from snowpack internal interfaces (P_{layers})

The mathematical formulations of these components are detailed in section 0.

Using the assets of both AltiDop and SMRT simulators, it is possible to simulate the global signal acquired over a snow surface. The simulation follows the same three major steps, as already described in section 6.1:

<u>**First step:**</u> A numerical scene is generated, comprised of different pixels representing scene facets

<u>**Second step**</u>**:** The signal backscattered by each scene facet is retrieved using equation n°2 (see section 0). For that purpose:
- **PFS** is computed by **AltiDop**, using radar equation 8, detailed in section 6.1
- **PFV** is computed by **SMRT**, using equation 3, detailed in section 0. For now the PFV signal remains constant within the footprint, meaning that it doesn't change from one facet to another.

<u>**Third step:**</u> The altimetry signal is constructed by adding the facets contribution to the corresponding altimetry waveform samples, according to:
- for the PFS signal: the facet/antenna distance (as explained in section 6.1)
- for the PFV signal: the facet/antenna distance + a time delay due to signal propagation into the snowpack.

Figure 19 illustrates the AltiDop/SMRT simulation. In contrast with Figure 18, the signal backscattered by each facet is not a Dirac signal anymore, but integrates the volume contribution from SMRT. The signal displayed in Figure 19 follows an exponential decrease over time, which is simplified representation. Nonetheless it illustrates quite fairly the rapid decrease of the signal intensity along the snowpack depth.

FORM-NT-GB-7-1

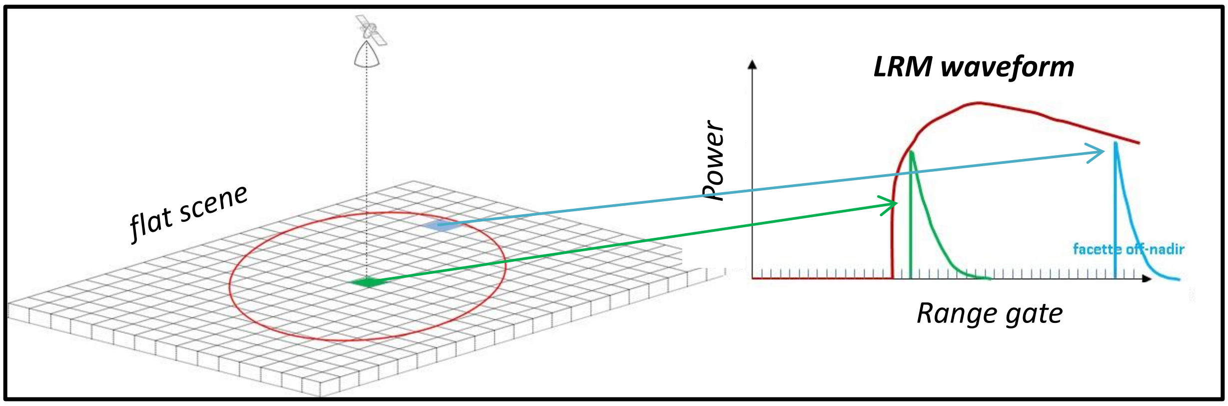

Figure 19: Illustration of the waveform generation over a snow surface with the AltiDop/SMRT coupling. The green and blue signals depict the signal backscattered by each facet. The volume contribution is illustrated here as an exponential decrease.

The Figure 20 shows the general operating scheme of the AltiDop/SMRT simulator:

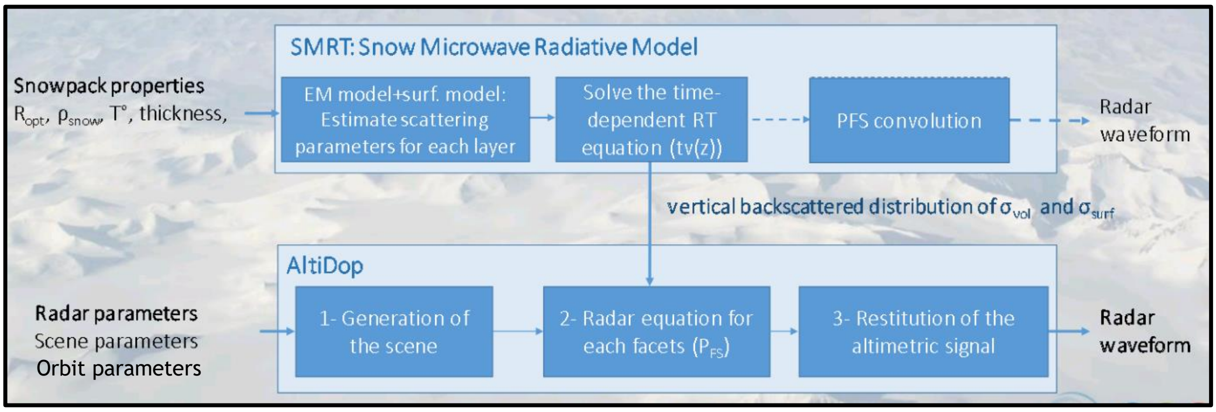

Figure 20: General operating scheme of the AltiDop/SMRT coupling

As represented in the diagram above and detailed in section 0, SMRT can generate altimetry waveforms itself, without AltiDop. For that purpose, a module was implemented in SMRT to simulate the PFS signal using the Brown formulation. Considering that PFV signal is assumed to remain constant at any satellite incident angle (in the 0° – 0.6° range), the simulation of the final altimetry signal can be performed by a simple numerical convolution between PFS and PFV. In that fashion, SMRT is able to simulate altimetry waveform when the surface is flat.

This is an alternative way compared to the approach using the AltiDop / SMRT coupling, for which the altimetry signal is computed using a numerical loop along the PFV signal (over time), to associate the PFV energy at the adequate waveform sample. Note that using a numerical facet simulator such as AltiDop bring some advantages. For instance, it is possible to change or add surface roughness, surface slope, backscattering heterogeneities, PFV variations… within the radar footprint, to simulate multiple case studies. AltiDop also brings the advantage to simulate SAR model waveforms, or complex pulses in I & Q.

6.2.2. Validation

To validate the AltiDop and SMRT coupling, two simulations were carried out:

- A simulation with SMRT alone, using a numerical convolution between PFV and PFS (from Brown model)
- A simulation with the AltiDop/SMRT simulator, over a perfectly flat scene

The Figure 21 shows the comparison of the simulated waveforms. **The excellent agreement between both simulations validates the developments made.**

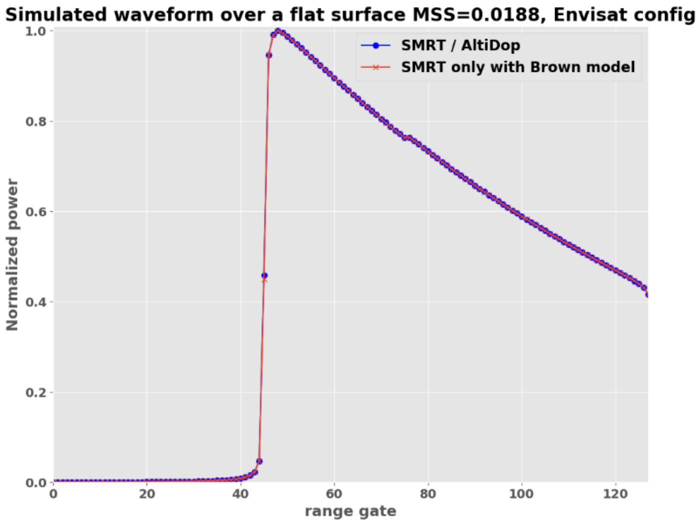

Figure 21: Comparison of LRM waveforms using AltiDop/SMRT coupling (blue) and SMRT only with PFS from Brown model (red)

7. Performance analysis over ice sheet

7.1. Reference snowpack definition

Before beginning the performance study, it is first necessary to define a reference snowpack, around which we will study the sensitivity of the altimetry measure to snow and topographic parameters. Without any precise snow in-situ measurements available yet, we have two options for defining a reference snowpack:

- By directly using the snowpack from Lacroix et al. (section 4.2)
- By tuning the snowpack parameters to get waveform shapes consistent with real acquisitions.

To evaluate both methods, we compared the simulations with real modern acquisitions made by different altimeters over lake Vostok. In fact, the large and flat surface of lake Vostok (~15 000km^2, surface slope ~0.0025%) is an ideal calibration site for altimetry. The flat surface prevents from topographic effects that can also modify waveform shape. The lake Vostok waveforms are well characterized from recent studies made at CLS, in LRM/SAR and Ku/Ka bands [Aublanc et al., 2017], and are displayed in Figure 22 (left column).

After running first simulations with the snowpack from Lacroix et al., we noticed that the modelled waveforms were relatively far from lake Vostok altimeter acquisitions. We have not investigated the profound reason of this disagreement. However, the snowpack from Lacroix was build to fit simulations to observations. Modeling errors were detected by IGE that could lead to wrong snow parameters retrieval.

We decided to slightly tune the snowpack parameters to generate more realistic waveforms. In fact, without realistic simulations the performance analysis does not make any sense, as the altimeter range derived from waveforms at level-2 is very sensitive to the waveform shape, in particular at the waveform leading edge.

First sensitivity studies conducted by IGE show that the main parameters acting on the waveform shape over ice sheets are the density, the snow grains size and the mean square slope. To define the reference snowpack the following methodology was taken:

- **Density is set at 320 kg.m^{-3}** , which is for instance the averaged surface density at Dome C [Picard et al. 2014]

- We search [snow grain size ; mean square slope] realistic couple of values that reproduce fairly the waveforms shape measured over lake Vostok:

  - ⇨ For the snow grain size parameter, simulations were performed with varying values for a radius between 100µm and 500µm.

  - ⇨ The Mean Square Slope (MSS) over snow is not very well referenced in the literature. Nonetheless, nadir MSS can be theoretically computed using the following equation:

$$MSS = \frac{|R(0)|^2}{s^0}$$

With $|\boldsymbol{R}(\mathbf{0})|^2$ being the Fresnel coefficient, with a value expected around ~0.15 over snow [Davis et al. 1993].

*With $\boldsymbol{s}^{\mathbf{0}}$ being the radar backscattering coefficient. It is not straightforward to find a realistic value for lake Vostok. From the literature [Remy et al., 2009], we get a ~5dB value over lake Vostok, leading to a **~0.007** mean square slope. (Note that the 5dB value integrates the whole energy, from surface and sub-surface, so the s^0 at snow/air interface should be lower).*

FORM-NT-GB-7-1

⇨ Finally, regarding the parameter uncertainty, a relatively large range of variation was chosen for the mean square slope: from 0.001 to 0.05.

At the end, the final reference single-layered snowpack was defined using the following snow parameters:

- **Density = 320 kg.m^{-3}**
- **Snow grains radius = 225µm**
- **Mean square slope = 0.03**

Figure 22, right column, shows the simulated waveforms in:

- LRM Ku band (top), CryoSat-2 configuration
- SAR Ku band (middle), Sentinel-3 configuration
- LRM Ka band (bottom), AltiKa configuration

All the simulated waveforms are very consistent with real acquisitions made over lake Vostok (left column). In particular the simulated LRM Ku-band waveform (green) reproduces well the leading edge inflection observed at mid-power. In LRM Ka band (red), volume scattering has relatively low impact on the waveform shape, neither in simulation nor in the real data, as expected. In SAR Ku band (blue) the volume effect can be observed in the trailing edge, and simulated/real waveforms are comparable. Nonetheless, the SAR Ku simulated waveform is slightly peakier, suggesting that there is room for improvement, in particular for snow / radar wave interactions at the very top of the snowpack. Besides, it could also be a limitation of using a homogeneous snowpack, neglecting the snow parameters vertical variations.

This reference snowpack was empirically built, using the AltiDop/SMRT model not yet fully validated. We are aware that is not the best and proper way to define the reference snowpack of the study. Nonetheless, without precise snow and roughness in-situ measurements this was the best approach we could take within the available time of the study.

A clear evaluation of the AltiDop/SMRT model will be mandatory to characterize its validity. Such an evaluation must be performed with snowpacks built with in-situ measurements. Then the simulated waveforms would have to be compared with real acquisitions take over in-situ measurements. Such a study was out of the scope of this study.

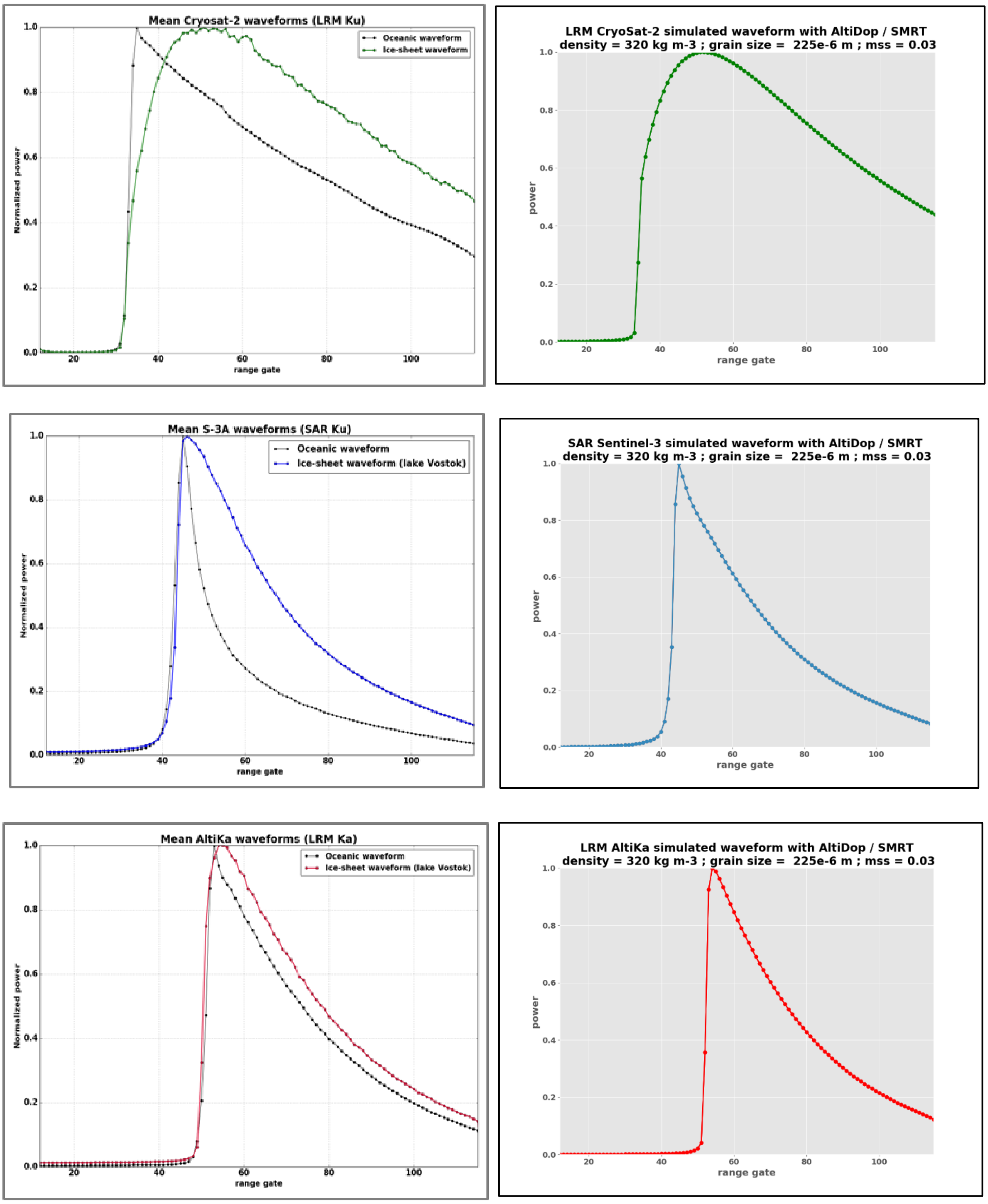

Figure 22: (Left column) Mean measured waveforms over lake Vostok (colored) and ocean (black) ; (right column) simulated waveforms using AltiDop/SMRT.

7.2. Level-2 parameters

In this study we assess the altimetry waveform sensitivity to snow parameters and surface slope variations. To quantify and evaluate the impacts of these parameters on the altimetry measure, several geophysical and waveform shape parameters are retrieved using simple level-2 retracking methods:

- The **surface elevation** using a threshold relative to the waveform maximum energy. This is a method classically used by the community, for example in the Threshold First Maximum Retracking Algorithm (TFMRA) [Helm et al., 2014]. The computation is relatively straightforward as the waveform is simulated with nadir/poca surface elevation return positioned at gate 44 exactly.
- The **air/snow threshold** to derive the exact surface elevation, at snow/air interface.
- The **leading edge width**, a parameter introduced with the ICE-2 algorithm [Legresy et al., 2005], used in the ENVISAT and AltiKa ground segments. Here it is computed between [10% – 100%] of waveform maximum power.
- The **pulse peakiness**, a classical waveform shape parameter, defined as the ratio between the waveform maximum energy and waveform mean energy (here it is computed over [12-115] waveform samples). It characterizes how specular the waveform is. **Only computed in SAR mode for this study, as it is less relevant in LRM.**
- The **backscattered energy, relative to the waveform reference snowpack (in dB)**. As the simulator is not yet capable of delivering realistic energy values, there is still the possibility to analyze the backscattered energy by comparison to a nominal configuration. In this study, this value is computed as follows:
  - Waveforms are normalized to the reference snowpack waveform
  - The relative backscattering energy is then computed as follows:

$$\theta r\ (dB) = 10 * \log \frac{Px}{Pref}$$

with Px maximum power of the analyzed waveform
with Pref maximum power of the reference waveform

The Figure 23 illustrates some of the parameters presented above in a SAR altimetry waveform: the leading edge width (blue), the air/snow threshold (red), the surface elevation at 50% of maximum power (green):

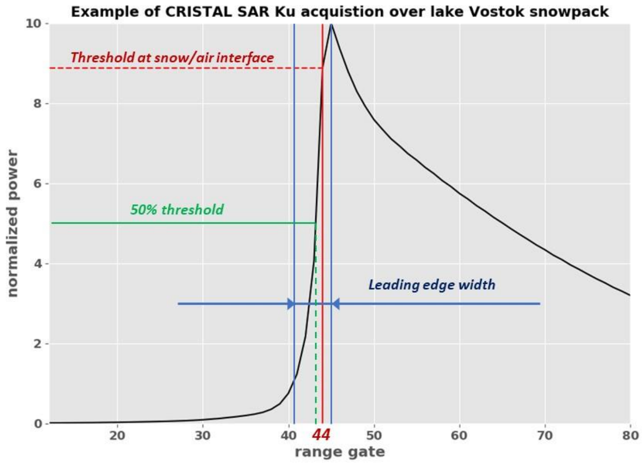

Figure 23: Illustration of the level-2 parameters analyzed in this study.

The simulations are configured according to the planned CRISTAL instrumental configuration, and the planned chronogram for ice sheets, which will be SAR closed-burst in Ka band and SARIn closed-burst in Ku band. Below are the main instrumental/orbital parameters employed for the CRISTAL configuration:

- Frequency = 35.75GHz in Ka band / 13.5GHz in Ku band
- Bandwidth and sampling = 500 MHz
- Pulse length = 49µs
- Antenna aperture = 0.43° in Ka band / 1.04° in Ku band
- Antenna gain = 50.1dB in Ka band / 42.1 dB in Ku band
- Pulse Rate Frequency = 18kHz
- Burst Rate Frequency = 80Hz
- Pulses per burst = 64
- Burst per 20Hz radar cycle = 4
- Satellite altitude = 800km (arbitrary choice, same as Sentinel-3A)
- Reference gate = gate 44 (arbitrary choice, same as Sentinel-3A)

7.3. CRISTAL simulated waveforms with the reference snowpack

Figure 24 shows the LRM waveforms simulated with the AltiDop/SMRT numerical tool using the ice sheet reference snowpack. *The PFS waveforms from AltiDop are also displayed in dotted line for comparison, corresponding to the signal at snow/air interface (no volume scattering).*

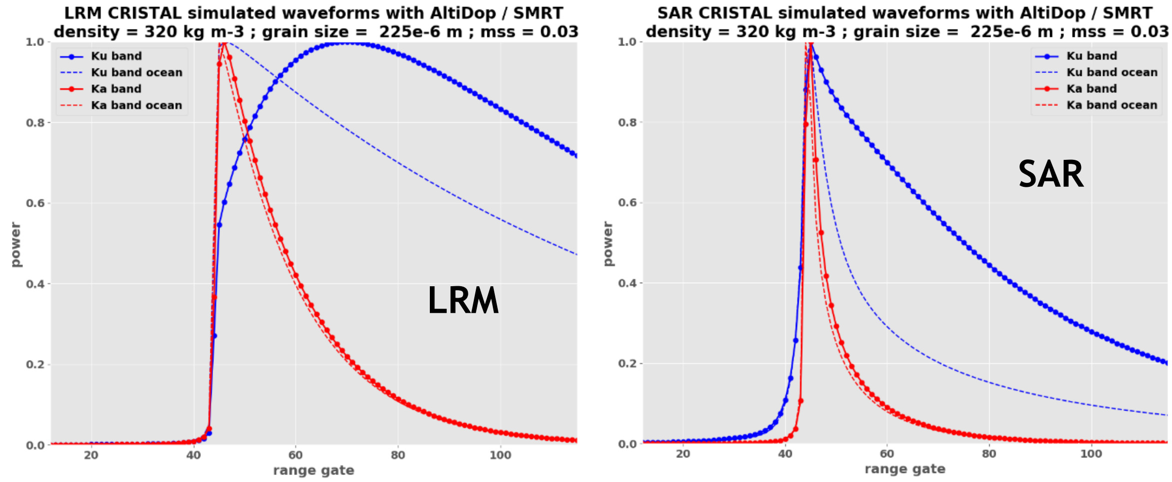

Figure 24: CRISTAL simulated waveforms using the AltiDop/SMRT simulator, in Ku band (blue) and Ka band (red), in LRM (left) and SAR mode (right). Oceanic waveforms from AltiDop are also displayed in dotted line.

The waveform leading edge obtained in LRM Ku band is very curved, rounded, with a clear inflexion positioned around leading edge mid-power. This is consistent with measurements taken by conventional altimeters. On the other hand, the leading edge in LRM Ka band is visually not impacted by volume scattering, as observed with AltiKa measurements.

To analyze more precisely the SAR measurements, Figure 25 presents the corresponding 2D stack simulated:

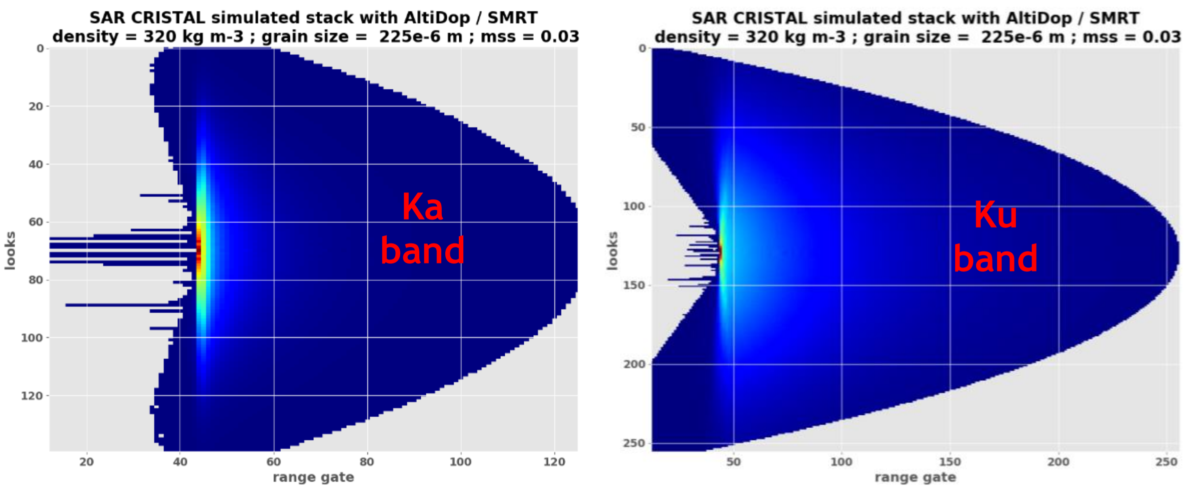

Figure 25: CRISTAL SAR stack simulated in Ka band (left) and Ku band (right) using the ice sheet reference snowpack

CRISTAL is planned to acquire waveforms in 1024 range gates, which is a long window analysis, 4 times longer than Sentinel-3A one for instance. Nonetheless, to reduce the important simulation CPU time in SAR mode, data were simulated with an optimized number of range gates:

- **In Ka band**, due to the narrow antenna aperture (0.43°), **128 range gates** are sufficient to capture the antenna pattern useful energy. At the end, there is approximately **80 useful looks**, that contain enough energy to efficiently reduce speckle noise during the multi-looking operation.

- **In Ku band**, the antenna aperture is wider (1.04°), therefore **256 range gates** were used to capture the antenna pattern useful energy. There is approximately **160 useful looks** that contain enough energy to reduce speckle noise. The ratio of useful looks between Ku and Ka bands is relatively comparable to the antenna aperture ratio of both antennas.

(we considered looks as "useful" when their maximum energy reach ~10% of the central looks energy.)

In the end SAR Ka band waveforms appear to be highly peaky, due to the specific SAR sampling, and the narrow antenna aperture. In Ku band the SAR waveform shape is much more "volumic" because of the larger antenna aperture, but mainly because of the volume scattering effect. It is clearly noticeable when comparing oceanic and ice sheets waveforms in Figure 24.

7.4. Performance analysis presentation

The performance analysis is divided in several parts:

- The section 7.5 presents plots of the waveforms simulated with varying snow parameters (density, grain size and mean square slope)
- The section 7.6 includes the variation of the estimated level-2 parameters
- The section 7.7 presents analyzes made with a varying surface slope
- Finally, the appendix C contains table of surface elevation biases, at different retracking thresholds, with varying snow parameters.

7.5. CRISTAL waveforms with varying snowpack parameters

7.5.1. Sensitivity to snow density

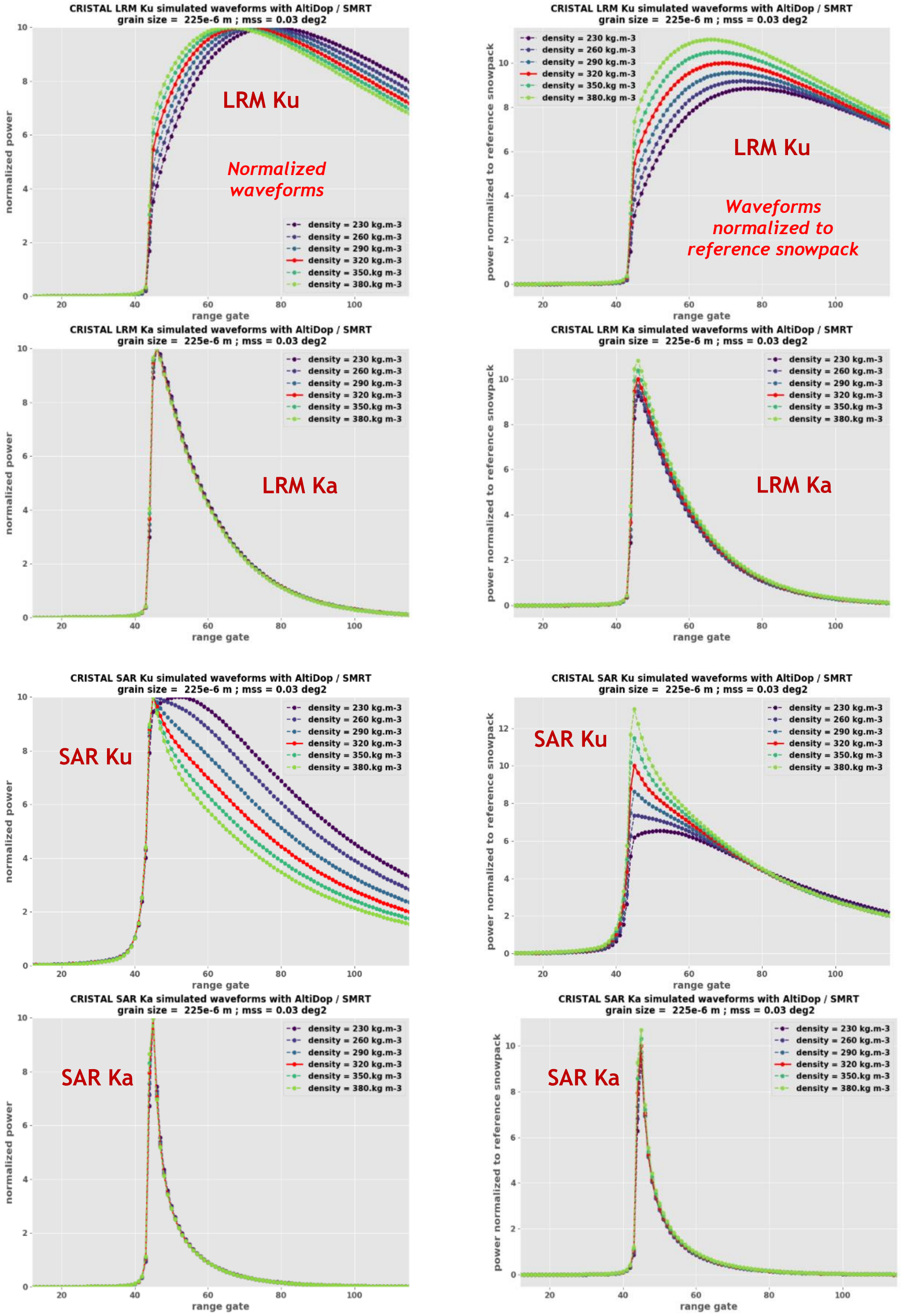

Figure 26: CRISTAL altimetry waveforms simulated with different snowpack density values, in LRM Ku band (top), LRM Ka band (2nd row), SAR Ku band (3rd row) & SAR Ka band (bottom). Waveforms are normalized by their maximal energy (left column) & by the reference snowpack waveform maximal energy (right column)

7.5.2. Sensitivity to snow grain size (with values corresponding to grain radius)

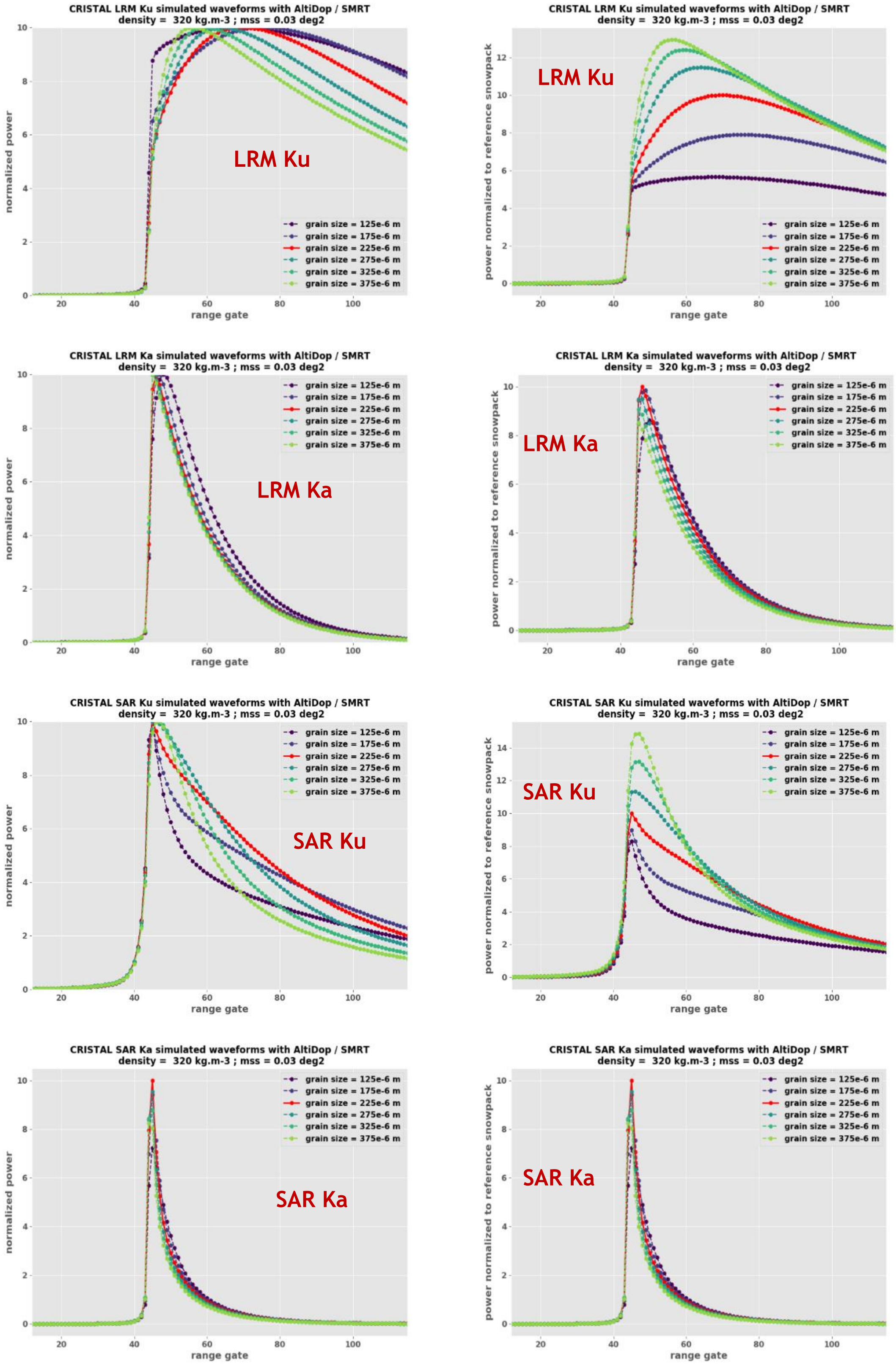

Figure 27: CRISTAL altimetry waveforms simulated with different different snow grain radius values, in LRM Ku band (top), LRM Ka band (2nd row), SAR Ku band (3rd row) & SAR Ka band (bottom). Waveforms are normalized by their maximal energy (left column) & by the reference snowpack waveform maximal energy (right column)

7.5.3. Sensitivity to mean square slope

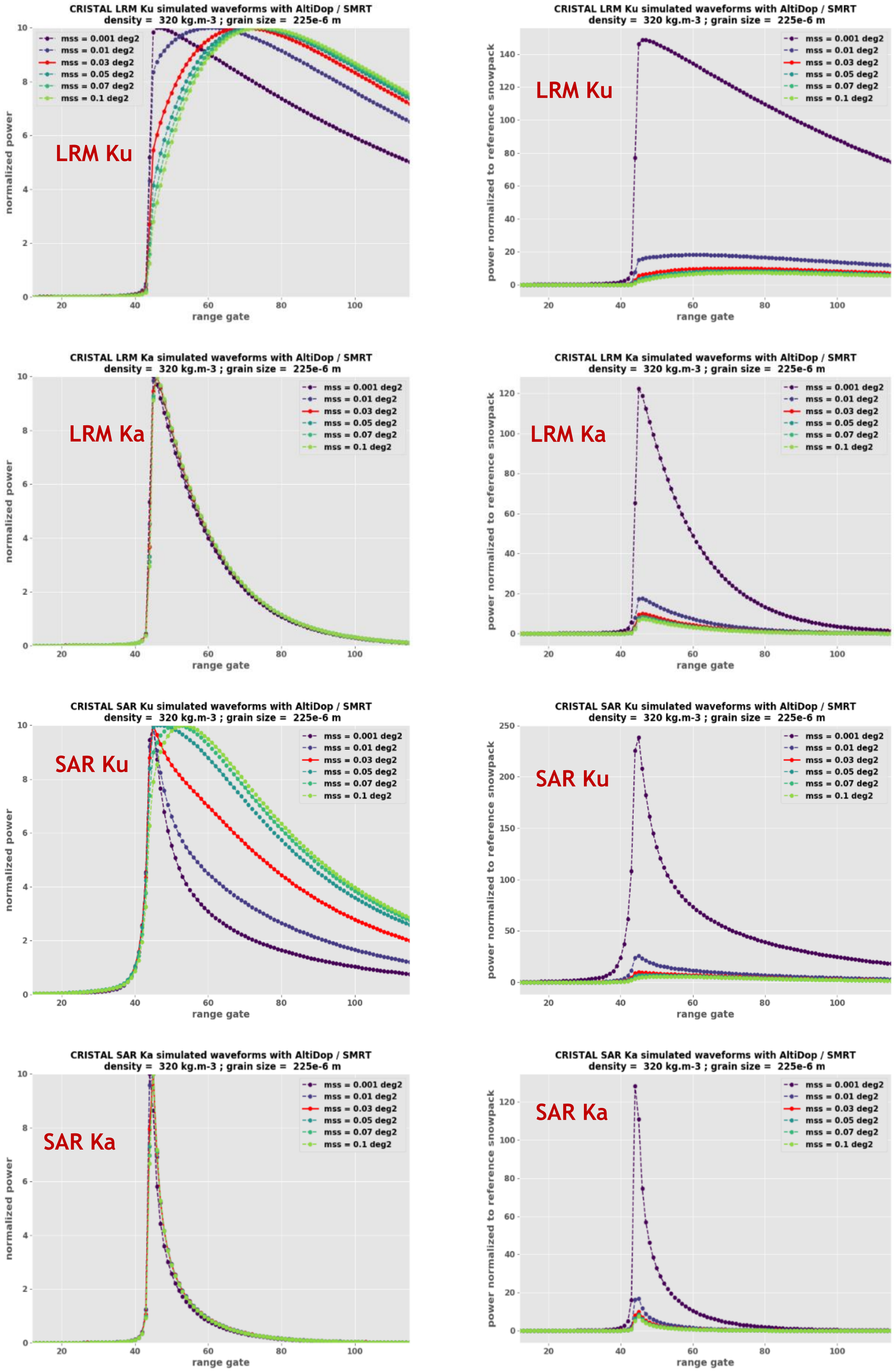

Figure 28: CRISTAL altimetry waveforms simulated with different mean square slopes values, in LRM Ku band (top), LRM Ka band (2nd row), SAR Ku band (3rd row) & SAR Ka band (bottom). Waveforms are normalized by their maximal energy (left column) & by the reference snowpack waveform maximal energy (right column)

7.6. Level-2 parameters sensitivity to snow parameters

7.6.1. Leading edge width

Figure 29 shows the leading edge width estimated, as a function of the snowpack density, grain size & mean square slope variations. The black vertical line indicates the value used in the reference single-layer snowpack configuration, presented in section 7.1.

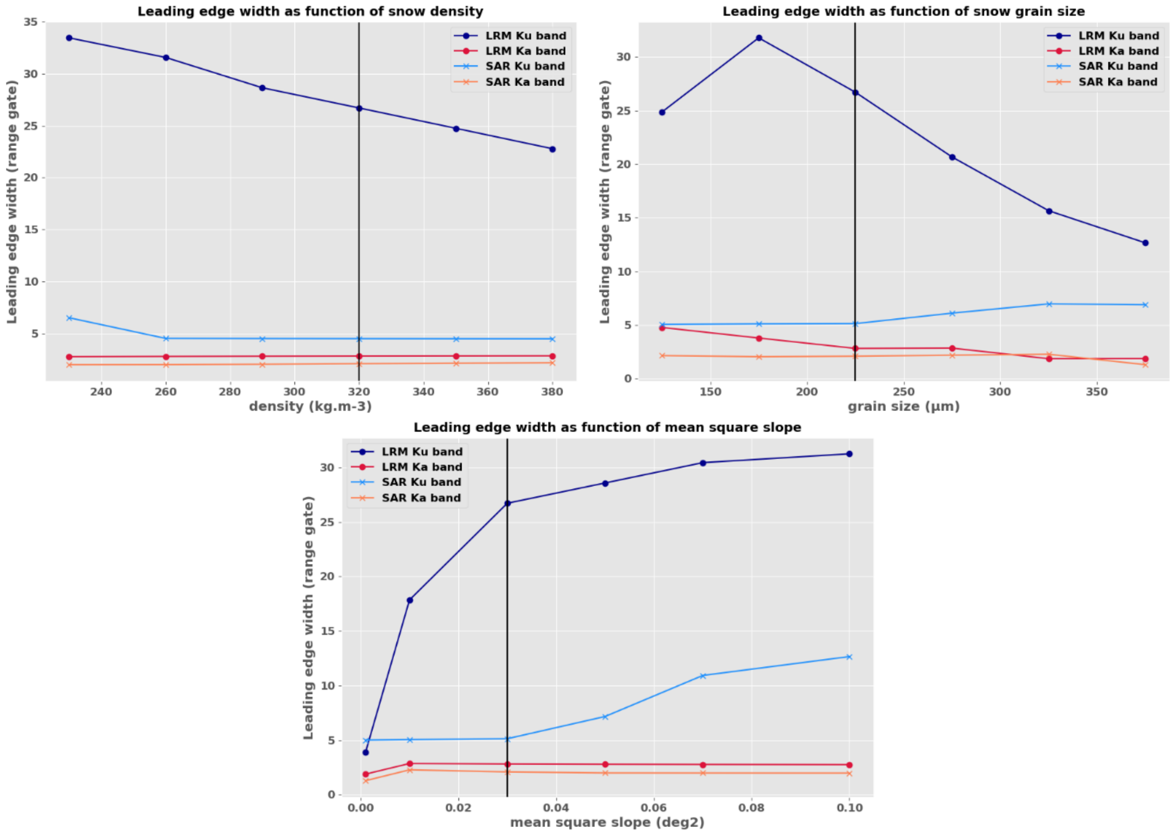

Figure 29: Leading edge width estimation as function of the snowpack parameters variations: density (top left), grain size (top right) and mean square slope (bottom). In CRISTAL LRM Ku (blue), LRM Ka (red), SAR Ku (cyan) and SAR Ka (orange).

Overall, in SAR mode Ku & Ka bands, the waveform leading edge width remains stable, whatever the parameter considered. Only exception, in Ku band, the waveform leading edge width increases for mss values higher than 0.03.

In contrast, in LRM Ku band the leading edge width is very sensitive to the three parameters studied, in particular to snow grain size. The most interesting configuration is the LRM Ka band, for which the waveform leading edge width is only sensitive to snow grain variations.

7.6.2. Backscattering energy

Figure 30 shows the backscattering estimation, relative to reference snowpack, and its sensitivity to snowpack density, grain size and mean square slope. The black vertical line indicates the reference single-layer snowpack configuration, presented in section 7.1.

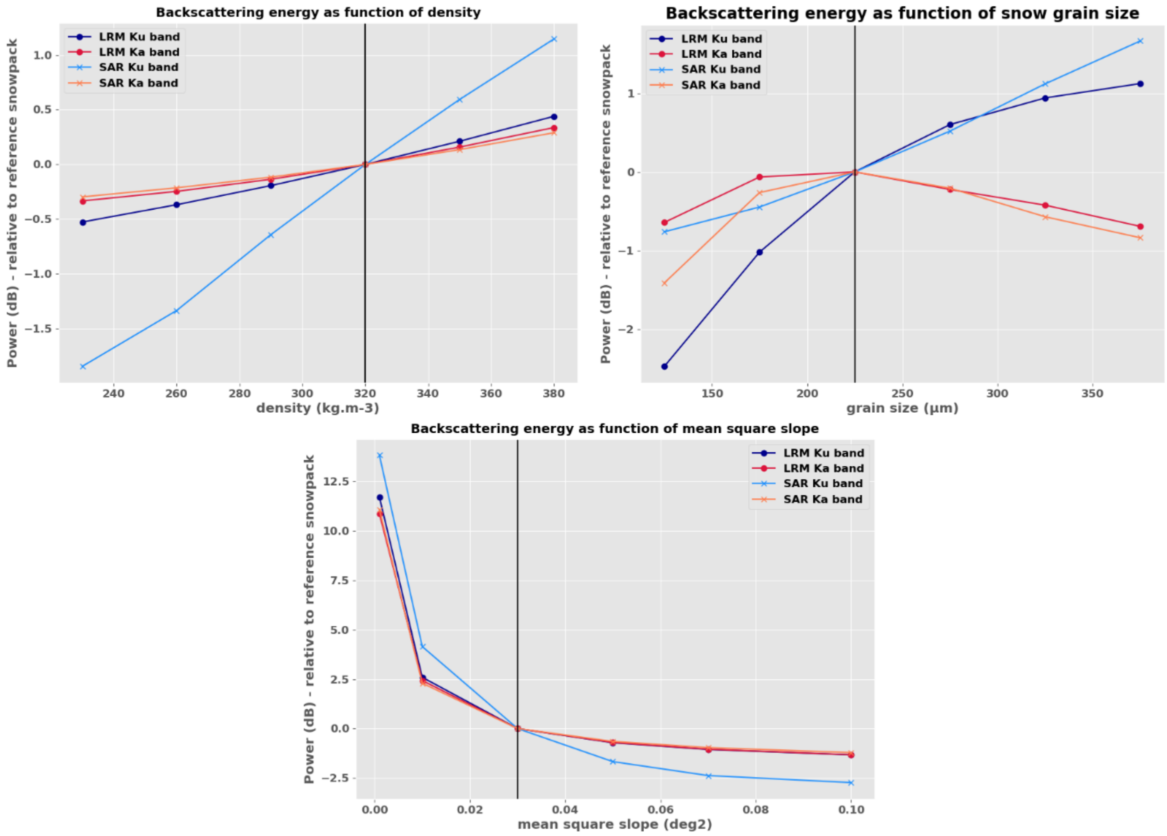

Figure 30: Backscattering coefficient estimation as function of the snowpack parameters, with varying density (top left), grain size (top right) and mean square slope (bottom). In CRISTAL LRM Ku (blue), LRM Ka (red), SAR Ku (cyan) and SAR Ka (orange).

Global trends show that backscattering coefficient raises when snow density increases, and mean square slope decreases. This is expected as both snow parameters variations make the air/snow interface return more prominent. In Ku band, backscattering coefficient raises when snow grain size increases. In Ka band, the backscattering sensitivity to snow grain size is more difficult to assess, with the highest energy obtained for grain radius between 175µm and 225 µm.

In Ka band, backscattering coefficient behavior is relatively equivalent in SAR mode and LRM. First results indicate that it is more sensitive to surface mean square slope, than density and grain size parameters. In particular, the backscattered energy rapidly increases when mean square slope is below 0.03 deg2. In Ku band, SAR mode the backscattering coefficient appears to be highly impacted by changes in snow density. This result was not expected and should be analyzed more deeply.

7.6.3. Pulse peakiness

Figure 31 shows the sensitivity of the SAR pulse peakiness to snowpack density, grain size and mean square slope. The black vertical line indicates the reference single-layer snowpack configuration, presented in section 7.1.

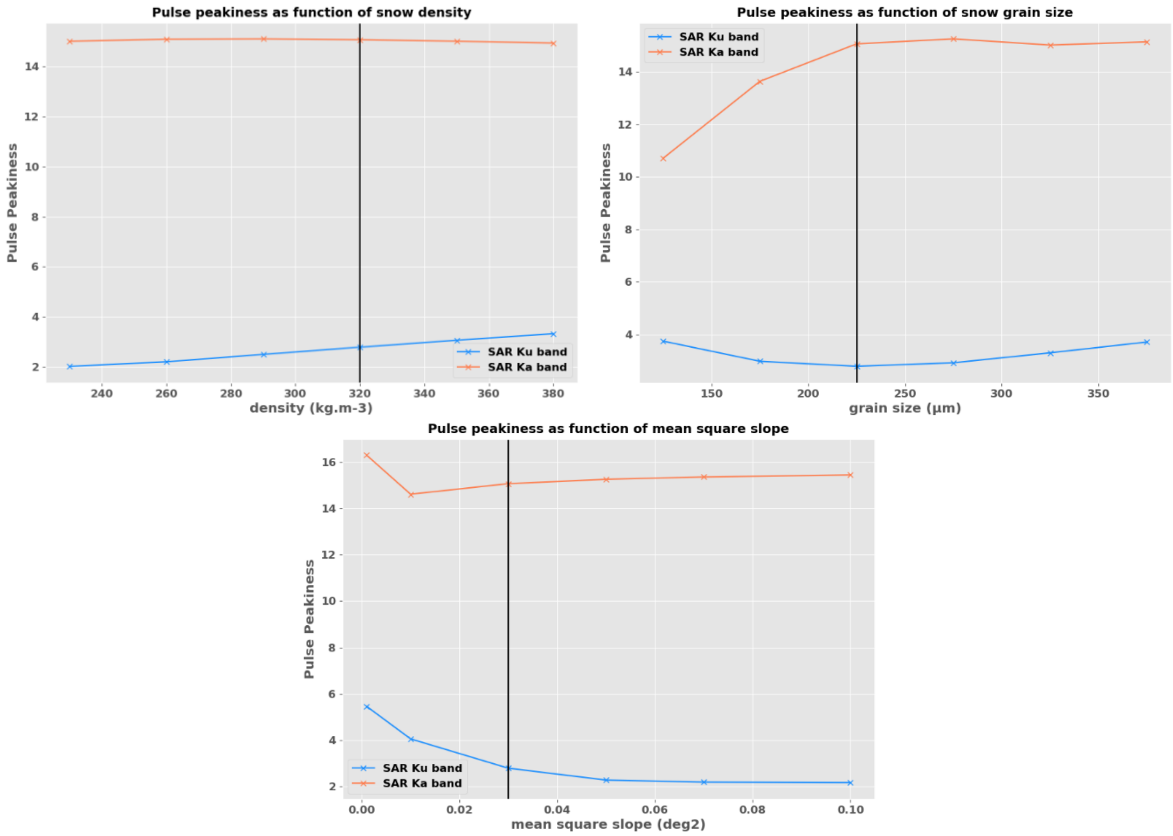

Figure 31: Pulse peakiness estimation as function of the snowpack parameters, with varying density (top left), grain size (top right) and mean square slope (bottom). In CRISTAL SAR Ku (cyan) and SAR Ka (orange).

In Ku band, pulse peakiness is sensitive to all snowpack parameters with a range of variations between 2 and 4 for the three snowpack parameters. On the other hand, in Ka band pulse peakiness rapidly decreases when the grain radius is below 225µm. Otherwise it remains relatively non-sensitive to density and mean square slope variations.

7.6.4. Retracking threshold at snow/air interface

Figure 32 shows the sensitivity of the air/snow retracking threshold to snowpack density, grain size and mean square slope. The black vertical line indicates the reference single-layer snowpack configuration, presented in section 7.1.

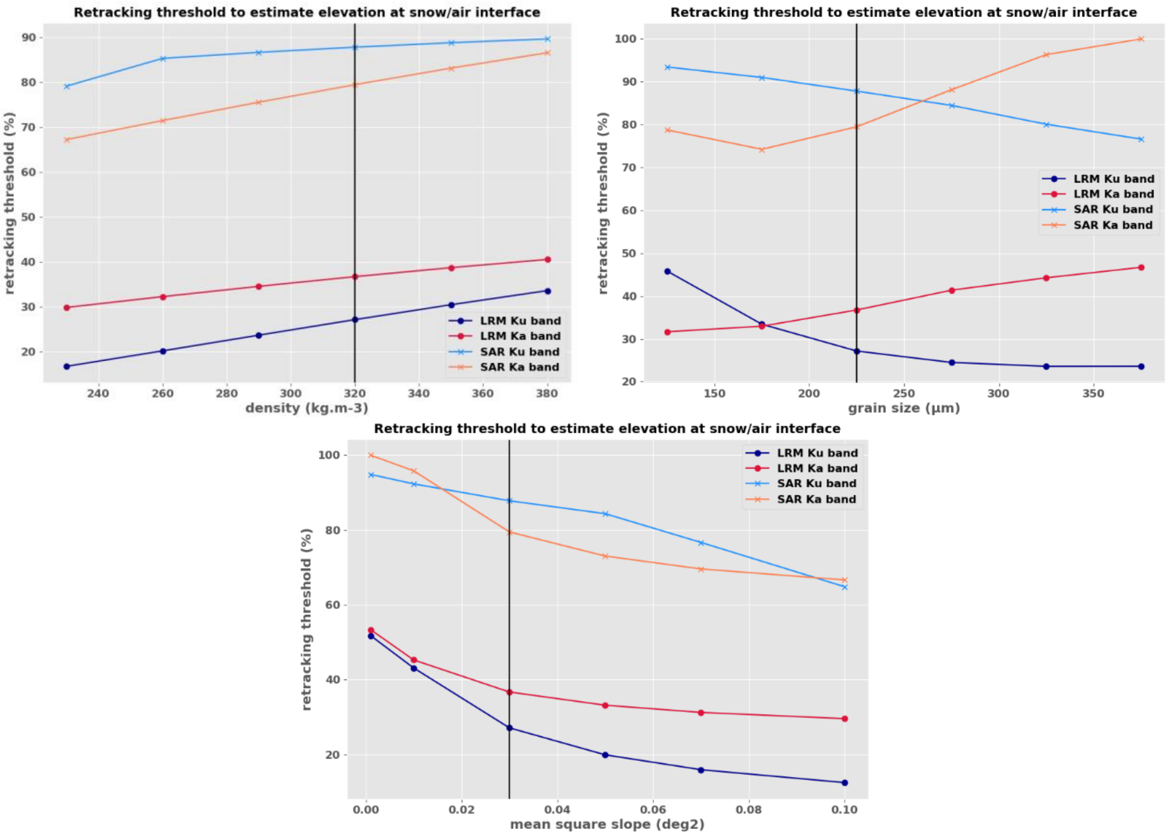

Figure 32: Air/snow retracking threshold as function of the snowpack parameters, with varying density (top left), grain size (top right) and mean square slope (bottom). In CRISTAL LRM Ku (blue), LRM Ka (red), SAR Ku (cyan) and SAR Ka (orange).

The following sensitivities are observed, for each of the analyzed snowpack parameters:

- **Density sensitivity:** For all configurations, the air/snow threshold rises when the snowpack density increases. In LRM, threshold amplitude variations are more important in Ku band compared to Ka band, but the opposite is observed in SAR mode.
- **Grain size:** Ku and Ka bands have two different behaviors. While an increase of the snow grain size lower the air/snow interface threshold in Ku band, it raises it in Ka band.
- **Mean square Slope:** As expected, an increase of the mean square slope induces a decrease of the air/snow retracking threshold

Overall, the figures above show that, for all configurations, the air/snow retracking threshold is sensitive to the three snowpack parameters studied. This is an important result as it exhibits that a level-2 retracker must account for these variations if its purpose is to estimate surface elevation at snow/air interface.

If still considering an empirical retracker (as TFMRA or OCOG retrackers), the strategy would be to retrack at a low position on the waveform leading edge to get a lower sensitivity to snowpack variations, with the counterpart of overestimating surface elevation. This is the current global strategy adopted for most of the level-2 algorithms at present.

Another strategy would consist in developing a physical retracker (based on a physical modeling of the snow pack), accounting for the main impacting parameters that have been discussed previously. Studies are needed to further exploit the simulation tool that has been developed and to define such a family of physical retracker that has never been developed before.

7.6.5. Conclusion

The sensitivity study performed with different CRISTAL configurations is very instructive and leads to the following main conclusions:

- The three parameters (density, snow grain size and MSS) have a significant influence on the global waveform shapes. In particular on the waveform leading edge, and at the end on the estimated surface elevation. This applies at different degrees in the 4 CRISTAL configurations that have been studied (LRM Ku, LRM Ka, SAR Ku and SAR Ka). It was not really anticipated that the snow/air retracking threshold in Ka band be as sensitive as in Ku band.

- We can anticipate that the different measurement configurations allowed by the CRISTAL dual band altimeter are highly valuable to discriminate snowpack variations. For instance, in these simulations:
    - SAR Ka band pulse peakiness parameter is only sensitive to small snow grain size.
    - SAR Ku band leading edge width is mainly sensitive to mean square slope
    - For all configurations the backscattered energy is high for low mean square slopes values

- It will be really relevant to refine this study with more realistic variations of the different parameters and values coming from in-situ data. This is particularly true for the mean square slope.

- Then, it will also be interesting to refine the reference snowpack, from single-layer to multi-layer as we anticipate that the leading edge and the snow/air interface threshold are sensitive to vertical variations at the snowpack upper part.

- Finally, it would be really relevant to define and develop a physical retracker (based on a physical modeling of the snow pack), accounting for the main impacting parameters that have been discussed previously. For that, studies are needed to:
    - further exploit the simulation tool that has been developed,
    - define such a family of physical retracker that has never developed before,
    - assess how the dual Ku/Ka measurements can discriminate the estimated parameters

7.7. CRISTAL sensitivity to surface slope

7.7.1. LRM

To illustrate the effect of surface slope in radar altimetry, a first example is presented in LRM, with a 1% surface slope applied. In this example the slope is simulated in the across-track direction, but it would have the same effect in the along-track direction, which is representative of the coastal regions in Antarctica. Figure 33 shows:

- The energy backscattered by the scene facets, computed from radar equation [9]
- The elevation of the scene facets. As we apply an across-track slope, the elevation increases in the across-track direction.
- The black mark corresponds to satellite nadir position. The white dotted lines correspond to the iso-range gates from 44 (leading edge) to 128 (end of the window analysis in this simulation)

<u>In this example a 1% across-track slope is applied.</u>

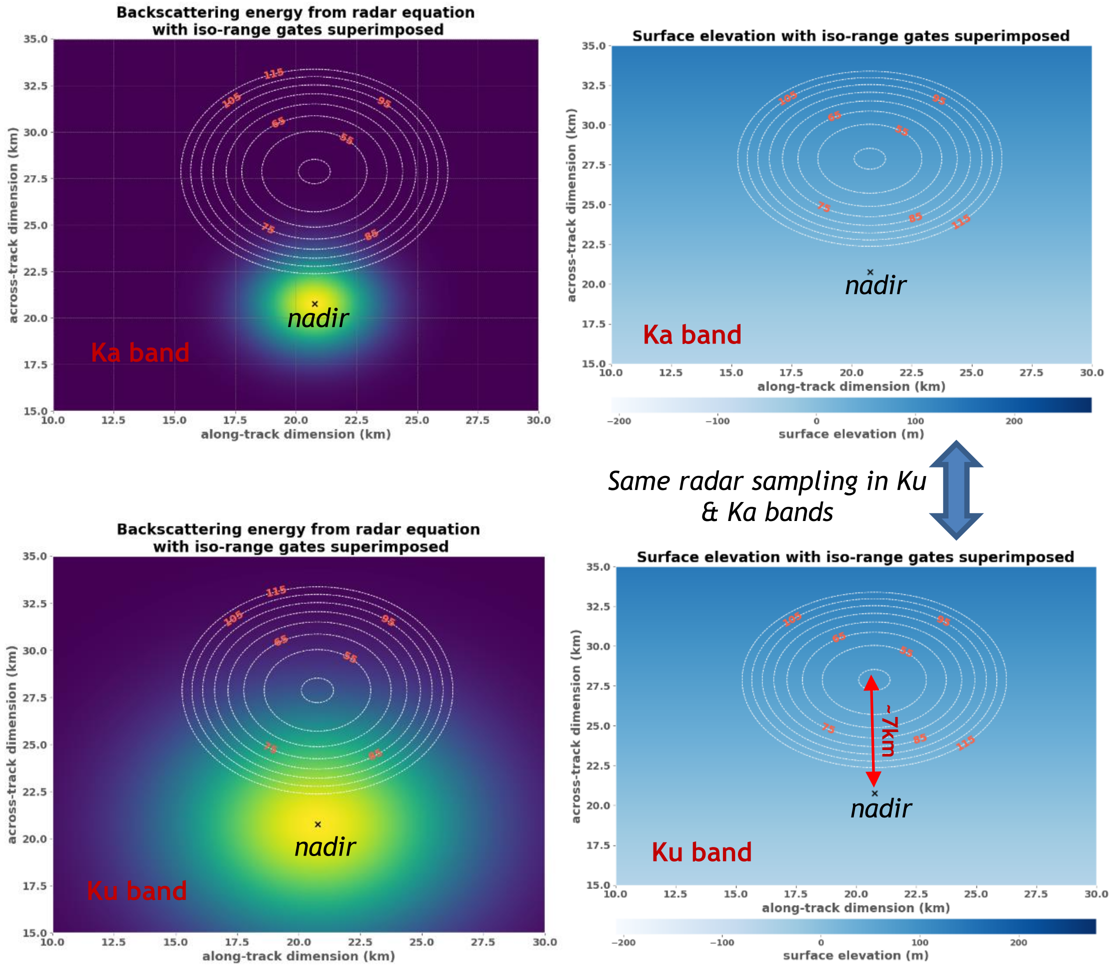

Figure 33: Energy backscattered by the facets (left) and facets elevation (right), in Ka band (top) and Ka band (bottom). LRM iso-range gates are displayed in white dotted lines, and satellite nadir is indicated with a black cross. In this simulation a 1% across-slope is applied to the surface elevation. Simulation is performed with AltiDOp/SMRT using the reference snowpack.

When a radar altimeter measurement is acquired over a non-flat surface, the first surface return originates at the Point Of Closest Approach (POCA). For a simple case of a linear surface slope, this corresponds to the orthogonal point between surface topography and satellite position. This effect is well known in radar altimetry and referenced as the “slope induced effect” [Brenner et al., 1983].

In the above example, with a 1% surface slope, the POCA is shifted upslope as illustrated by the white iso-range gates. In the simulation, the horizontal distance between nadir and POCA is approximately 7km. This is consistent with the theoretical computation given by Sandwell and Smith [2014]:

$$\Delta x = He * s^2 \qquad [9]$$

*With **He (m)** the effective altitude satellite given by He = H / (1+H / R) ; H being satellite altitude and R the Earth radius*
*And **s** the surface slope (%)*

This has a significant impact on the measured waveform. In particular, in Ka band, the first surface energy return is outside the -3dB antenna pattern, while in Ku band the POCA remains relatively illuminated. The Figure 34 displays the corresponding simulated waveforms:

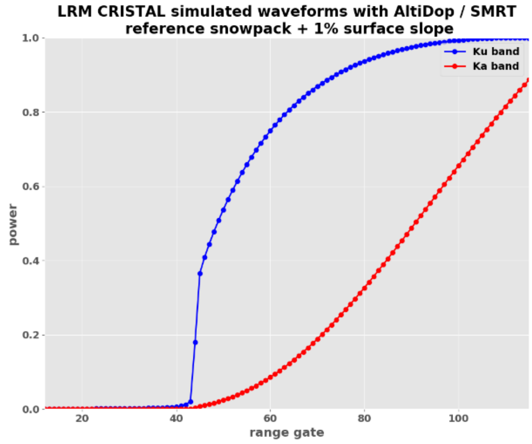

Figure 34: CRISTAL LRM waveforms simulated over a 1% surface slope from AltiDop/SMRT, and using the reference lake Vostok snowpack, in Ku band (blue) and Ka band (red)

As expected, the waveform shapes are distorted by the surface slope. In particular there is no clear leading edge in Ka band. In Ku band the surface elevation at POCA remains possible, but in this case the epoch must be estimated in the lower part of the leading edge (before 40% of waveform maximum energy). So the level-2 retracking algorithm must be capable to make such an adjustment.

Figure 35 shows **CRISTAL LRM waveforms, in Ku and Ka bands**, simulated over different surface slopes. For this simulation the satellite tracker was configured to follow the POCA, not the nadir, so the surface first energy returns stay measured at gate 44.

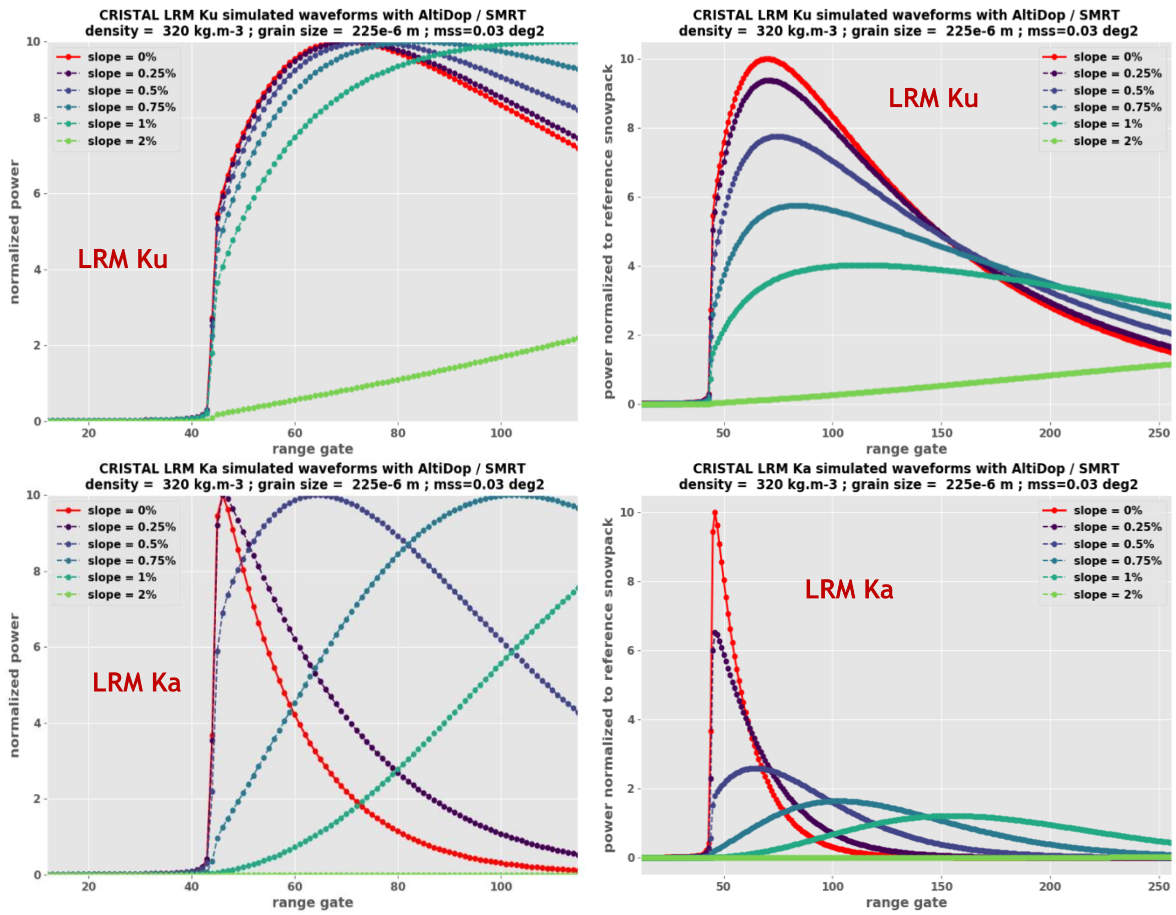

Figure 35: CRISTAL altimetry waveforms given different surface slopes, in LRM Ku band (top), LRM Ka band (bottom). Waveforms are normalized by their maximal energy (left column) and by reference snowpack maximal energy (right column)

Regarding the waveform shape it can be noticed that:

- In the normalized waveforms (left column), the trailing edge energy increases with the surface slope. In fact, the maximal antenna gain pattern is sampled by distant waveform range gates.
- The LRM Ku-band waveform leading edge remains relatively clear, noticeable, for a range of surface slopes between [0 – 1%]. With a 2% surface slope magnitude, the POCA is very distant from nadir, from approximately 28km. Therefore, there is no useful energy that can be sampled.
- In Ka band, the narrow antenna aperture emphasizes this effect, and the leading edge remains noticeable for a surface slope between 0 and 0.5%.

7.7.2. SAR mode

In SAR mode the problematic is different. The delay-Doppler processing generates a thin along-track sampling. With CRISTAL configuration, the signal measured originates from along-track Doppler bands, ~330 meters width in Ku band, ~100m width in Ka band. Therefore the measurement is not (or weakly) sensitive to along-track topographic variations, but the across-track sensitivity remains same as LRM [Aublanc et al. 2018]. Figure 36 shows CRISTAL SAR waveforms, Ku and Ka bands, simulated over several **across-track** surface slopes.

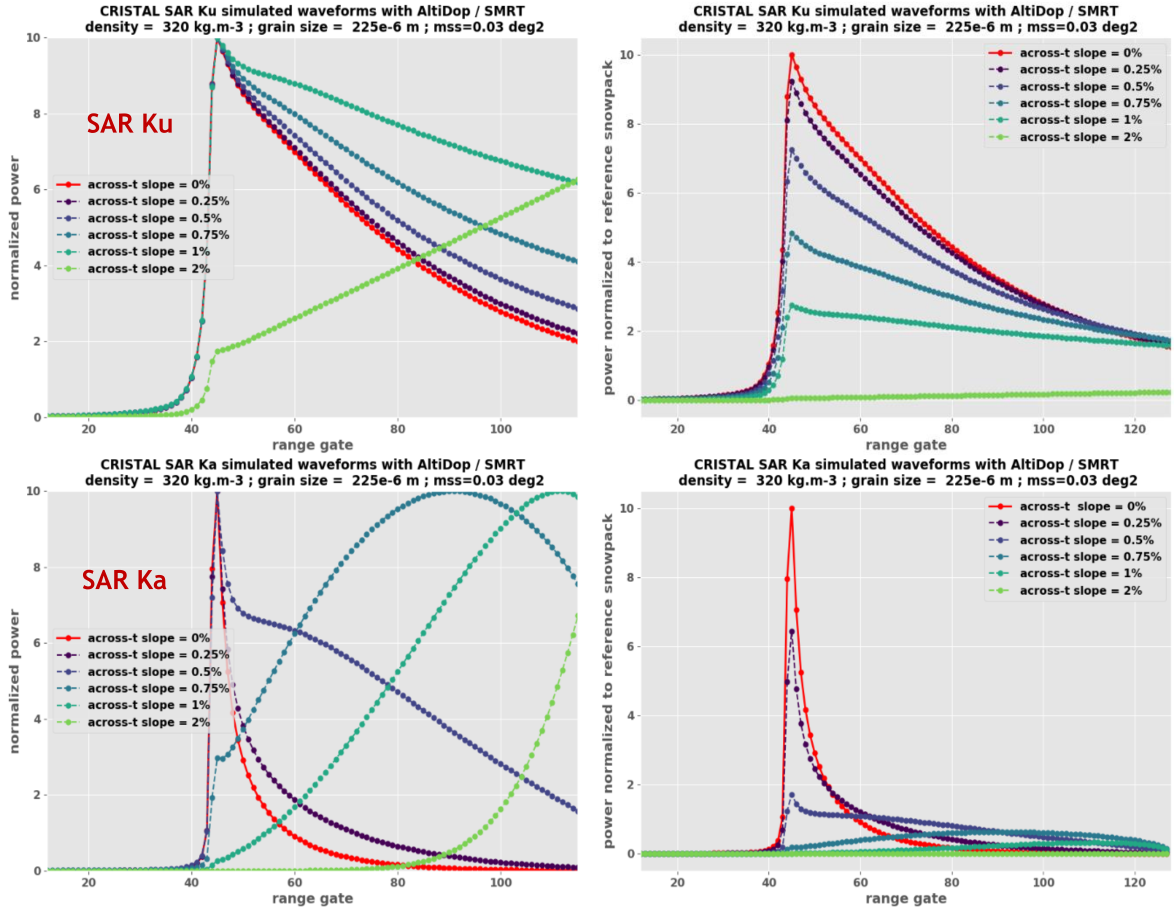

Figure 36: CRISTAL altimetry waveforms given different <u>across-track</u> surface slopes, in LRM Ku band (top), LRM Ka band (bottom). Waveforms are normalized by their maximal energy (left column) and by reference snowpack maximal energy (right column)

SAR mode sensitivity to across-track slope shows a behavior comparable to the one observed in LRM. In particular, when the across-track slope raises the energy backscattered at the leading edge is reduced and the energy sampled at the waveform trailing edge increases. Due to the peaky shape of the SAR waveform, the waveform leading edge remains a little less impacted compared to LRM measurements. In summary:

- **In SAR Ku band** the leading edge width remains constant up to 1% of across-track slope magnitude, which concerns a very large part of the Antarctic. For 2% of surface slope the measurement will be difficult to exploit at level-2, and backscattered energy is strongly attenuated.
- **In SAR Ka band** the leading edge width remains constant up to 0.5% of across-track slope magnitude, similarly to LRM.

Figure 37 shows CRISTAL **SAR waveforms, Ku and Ka bands**, simulated overdifferent **along-track** surface slopes.

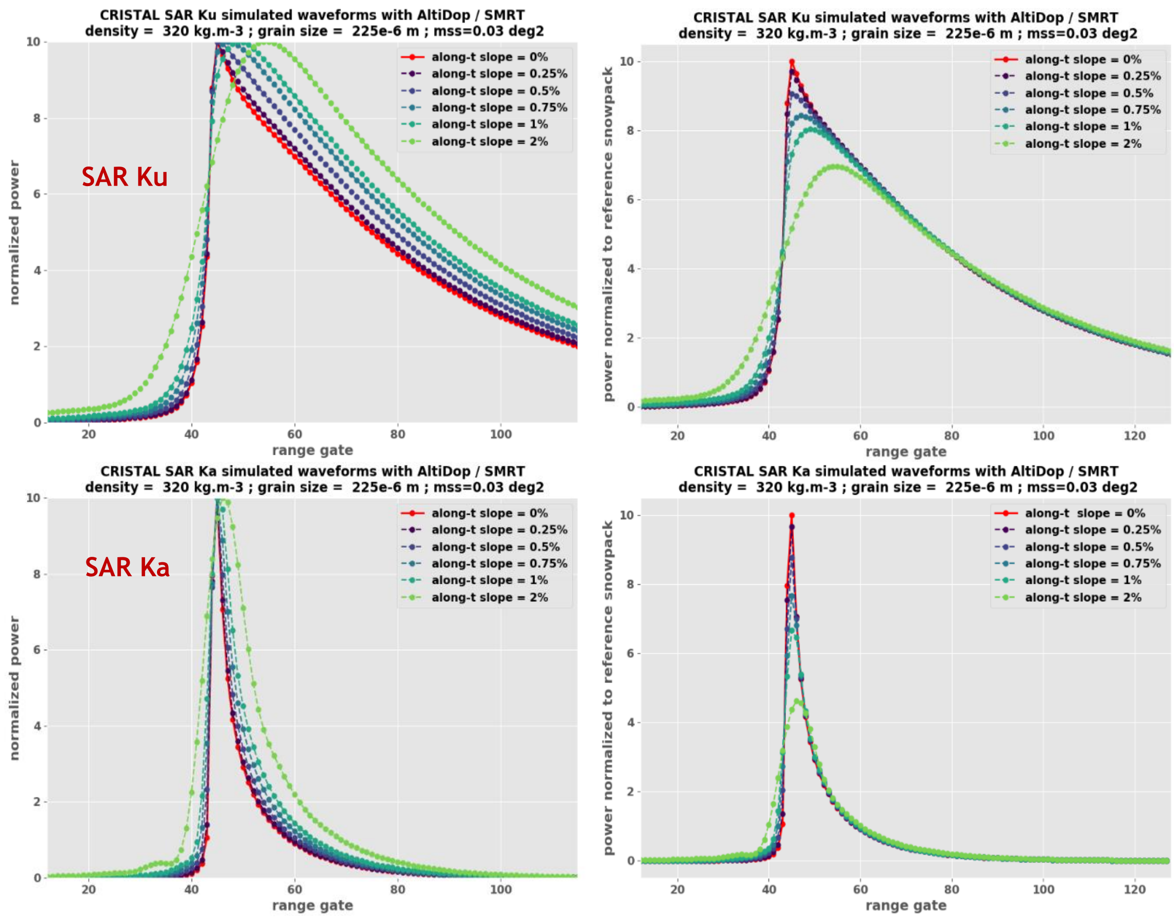

***Figure 37**: CRISTAL altimetry waveforms given different <u>along-track</u> surface slopes, in LRM Ku band (top), LRM Ka band (bottom). Waveforms are normalized by their maximal energy (left column) and by reference snowpack maximal energy (right column)*

As previously explained the SAR altimetry measurement is not or weakly sensitive to along-track topographic variations. As a corollary, the POCA remains located at nadir. And in fact, the simulations show that measurements remain relatively unchanged up to 2% of surface slope, in Ku and Ka bands. Nonetheless, a slight energy decreases is still observed when the along-track slopes raises. This is not expected and must be investigated in future studies. Moreover, the modification of the waveform shape needs to be understood and confirmed. It might be a realistic behavior, but also a limitation of the power simulation [I^2+Q^2]. Simulations performed with complex signal [I and Q], and using the same level-1 processing than ground segments (burst azimuth FFT in particular), could confirm the validity of these results. However, these kinds of simulations are more complicated to set up, and therefore require much more time than available for the present study.

7.7.3. Conclusion

We mainly anticipate two issues related to the surface topographic variations for the CRISTAL dual Ku/Ka altimeter:

- First, the measurement relocation performed at level-2 depends on the retracking method that has been employed. For instance, using a simple and constant retracking threshold leads to relocation biases, as we see that waveform leading edge shape changes with the surface slope magnitude. Methods have to be defined in order to quantify the biaises in a first time and then to avoid such biases in a second time. This is already an issue for current and past missions in LRM and SAR modes, as it is widely recognized that slope-induced error is the first source of error for altimetry over ice sheet.

- Second, we anticipate that Ku and Ka measurements could not always be co-located over a tilted surface. It probably happens over complex topographies, with rough surfaces at km scales. This would complicate the interpretation of the dual Ku/Ka measurements. Note that this is also strongly related to the level-2 retracking/relocation method that has been employed. To mitigate this aspect, the reduced footprint brought by SAR altimetry will necessarily limit the discrepancies between Ku and Ka estimated relocations.

7.7.4. Perspectives using high resolution DEM in simulation

The Reference Model Of Antarctica (REMA, Howat et al., 2019) is a new high resolution DEM of the Antarctica ice sheet. The DEM is built from stereographic images, registered with ICESat-1 and CryoSat-2, and provides the Antarctica topography with a 8 meters spatial resolution. First comparisons to in-situ data show excellent performances in term of accuracy and precision. The future registration with ICESat-2 will certainly provide even better performances. An equivalent version for Greenland ice sheet is also available.

Recently, and outside of the PolarMonitoring project frame, first promising results were obtained when combining AltiDop with the Reference Model Of Antarctica (REMA). In summary, the simulations were performed as follows:

1 – Instead of generating the scene inside AltiDop, the main idea was to take REMA as the surface elevation input
2 – The orbital information of a real altimetry track overflying the DEM is loaded. Two demonstrator tests were performed, with an AltiKa and a Sentinel-3A tracks. Both in (P)LRM.
3 - Power waveforms are simulated along the track using AltiDop classical operations
4 – The simulated waveforms are compared to real acquisitions

A first test was performed using AltiKa acquisitions from 2015. Figure 38 shows REMA tile used for this demonstrator, with AltiKa track overlayed:

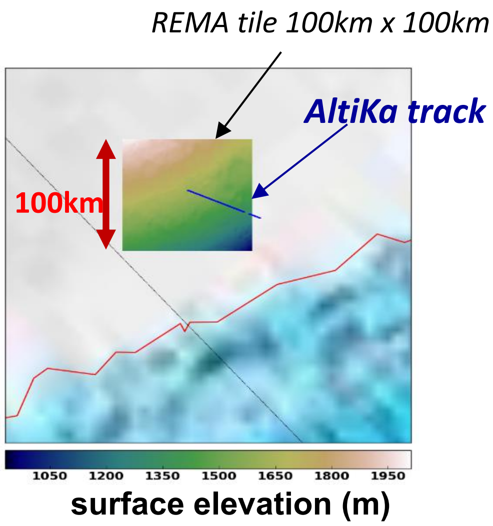

Figure 38: Location of the REMA tile used in a demonstrator simulation

Figure 39 shows the waveforms acquired by AltiKa (right) and the corresponding simulated waveforms (left).

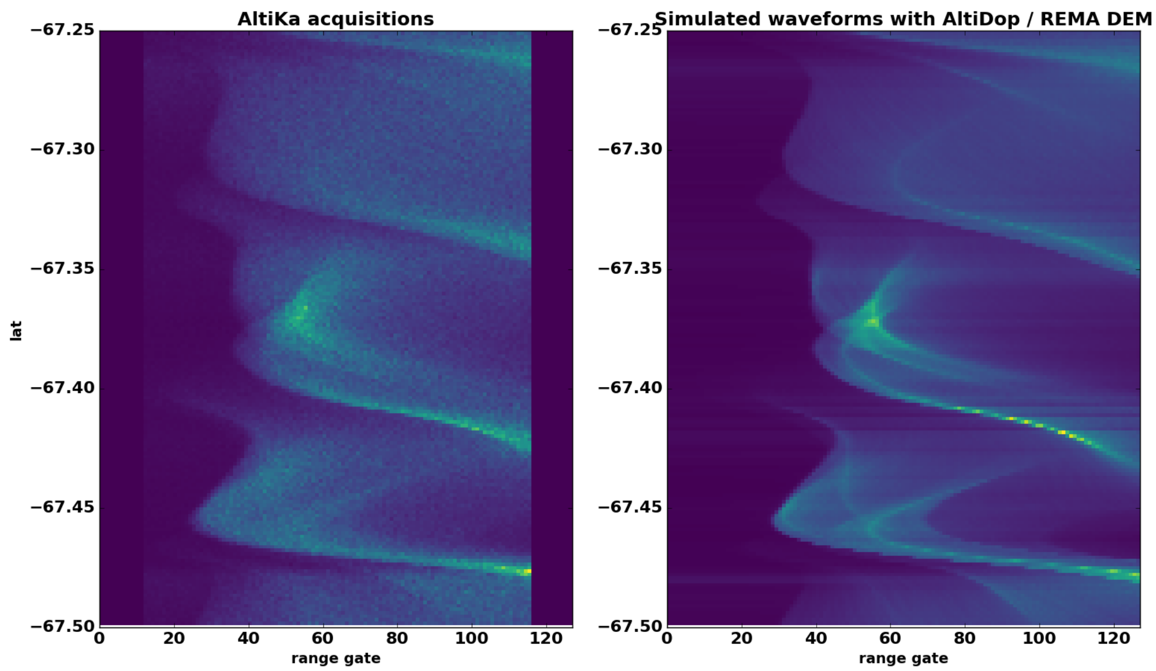

Figure 39: AltiKa measured waveforms (right) and AltiDop/REMA simulated waveforms (left)

Another test was performed over the same REMA tile using Sentinel-3A P-LRM acquisitions:

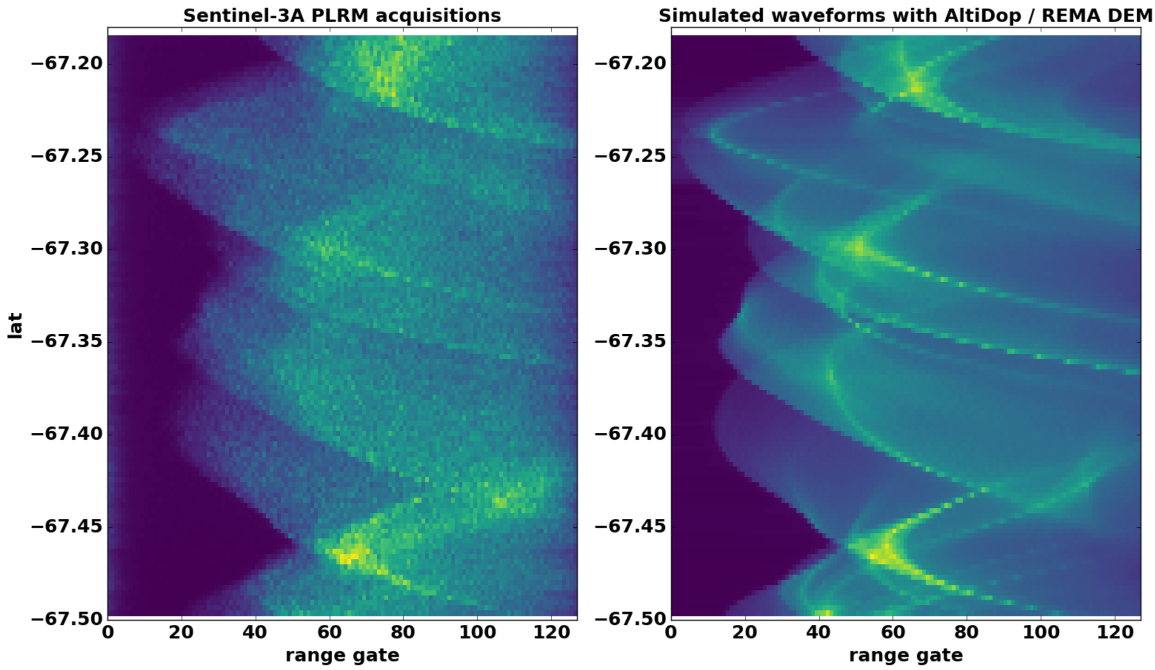

Figure 40: PLRM Sentinel-3A measured waveforms (right) and AltiDop/REMA simulated waveforms (left)

volume scattering from SMRT was not applied for both of these tests

The results are very promising and open new horizons for radar altimetry over the ice sheets. In particular, there is clearly the potential to improve the level-2 algorithms: both the retracking and the relocation methods. We will not go further into details here, as this is out of the scope of this project. In the frame of the CRISTAL mission preparation, using simulations with AltiDop/REMA has the potential to address several key problematics:

- To assess precisely the differences between Ku and ka measurements, in particular regarding potential colocation differences over complex topographies.
- To define the tracking instructions that will be used by the altimeter Open-Loop Tracking Mode on-board.
- To quantify the ice sheet area that can be successfully sampled by the CRISTAL altimeter, in both LRM and SAR modes and Ku and Ka bands. And conversely the area where topography is too steep/rough to be adequately measured.
- To assess influence of radar topography on the waveform shape, and how this can be handled at level-2 when estimating surface elevation and measurement relocation.

8. Conclusions and perspectives

An existing passive/active radiative transfer model (SMRT) originally developed by IGE, has been adapted by IGE for altimetry applications. With the new implementation, SMRT is now able to simulate the vertical backscattering distribution of a snowpack, which after convolution with the Brown model gives the LRM radar waveform. The model accounts for first order scattering only, which is valid in a domain which mainly depends on the frequency, snow grain size. The model is valid when the snow grain size is smaller than 0.8, 0.5 and 0.2 mm in the S, Ku and Ka bands, respectively. SMRT was validated by comparing simulations with the Lacroix et al. 2008's modeling, using the same configuration and inputs (normalized RMSE < 2%).

Then, SMRT was combined with the existing altimeter simulator (called "AltiDop") developed some years ago at CLS. Among other advantages, the coupling of the SMRT model and AltiDop enables to perform simulations for different surface topography scenarii (at a meter resolution scale). AltiDop is also capable of performing simulations in the SAR altimetry mode that will be available on CRISTAL. Two sensitivity analyses were conducted using single-layer synthetic snowpacks, theoretically representative of snow conditions observed over lake Vostok (Antarctica plateau):

- A first sensitivity study was conducted using the snowpack from Lacroix et al. [2008], in the AltiKa & Envisat altimeter configurations.
- In the second sensitivity analysis, the snowpack parameters are adjusted, in order that the simulated waveforms match with real acquisitions from CryoSat-2, AltiKa and Sentinel-3A. The sensitivity study was conducted with CRISTAL configurations, in LRM/SAR modes and in Ku/Ka bands.

The results of the two sensitivity studies are slightly different but reach the same major conclusions. The altimeter measurement is very sensitive to snow grain size, snow density and surface roughness at small scales (mean square slope). These three parameters act differently on the waveform shape, depending on the mode (LRM/SAR) and the frequency band (Ku/Ka). Therefore, we anticipate that a dual band altimeter such as CRISTAL would be highly valuable to discriminate the different geophysical parameters that modify the waveform shape over the snow surface. And subsequently to provide relevant information of the surface topography together with snowpack characteristics over ice sheets. The additional effect of the surface topography, at decimetric to kilometric scales, even more complicates the problematic by also modifying radar waveform shape. Nevertheless, new high resolution DEMs such as REMA bring promising solutions to understand and account for these topographic effects, in LRM and SAR mode.

An analysis of the surface slope effect was also conducted using CRISTAL altimeter configurations. As expected, the Ka measurement is more sensitive to surface slope when compared to Ku measurement, due to the narrower aperture of the antenna gain pattern (0.43° in Ka band vs 1.04° in Ku band, at -3dB). In SAR mode, Ka band, waveform leading edge remains consistent up to 0.5% of across-track slopes, which still concerns a very large part of the Antarctic continent. In SAR mode Ku band, waveform leading edge remains consistent up to ~ 1.5% to 2% of across-track slope. Moreover, the SAR mode brings the advantage to be not, or weakly, sensitive to the along-track slope, which will be very valuable over the ice sheet margins.

This prospective study brings promising results and we suggest undertaking the following actions:

1) To confirm and refine the conclusions reached in this study with an extended evaluation of the AltiDop/SMRT simulator. For that purpose, it would be necessary to define realistic synthetic snowpacks, built from in-situ snow measurements. The waveforms simulated using these snowpacks must then compared to real altimetry acquisitions overflying in-situ sites measurement. Such an analysis should ideally be conducted in LRM/SAR and in S/Ku/Ka bands.

2) Simulations performed with SMRT can be improved in Ka band (and lower frequencies) by taking into account 2nd order scattering. This could be done using a Monte Carlo technique to integrate the second and higher orders of scattering only, on top of the nadir_altimetry module which efficiently and accurately computes the first order. Progress have also to be made on the understanding of snow surface roughness and its impact in radar altimetry.

3) Regarding the ice sheet surface, sensitivity studies must also be conducted at global scales to account for the snow parameters variation over the whole Antarctica & Greenland continents. Seasonal variations of the snowpack geophysical parameters must also be studied.

4) Most of the results have been obtained for ice sheet surfaces. Sea-ice surfaces have to be investigated as well. Snow depth and freeboard estimations are among the main objectives of the CRISTAL mission. However, the lack of snow in-situ data over sea-ice prevents from precisely set the synthetic snowpacks. Once synthetic snowpacks will be defined, simulations have to be conducted as well to clearly identify the main impacting parameters and their range of variation.

5) A huge work has still to be done on level-2 algorithms. This first analysis demonstrates that the surface elevation derived from the waveforms is sensitive to several snowpack parameters (namely: snow density, snow grain size & mean square slope), for both LRM and SAR modes and both the Ku and Ka bands. Therefore, alternatives to empirical retrackers have to be carefully considered. We strongly recommend to define, develop and validate retrackers based on physical modeling of the backscattered signal. The number of parameters impacting the shape of the waveforms is great but we are confident that CRISTAL configuration, based on simultaneous Ku/Ka and LRM/SAR/InSAR modes, will provide enough measurements to discriminate/retrieve these parameters. This is the big challenge we have to face for the CRISTAL mission. Simulations must definitely help to do that job.

Appendix A - **References for section 2**

F. I. Adodo, F. Remy, and G. Picard, “Seasonal variations of the backscattering coefficient measured by radar altimeters over the Antarctic Ice Sheet,” *Cryosph.*, vol. 12, pp. 1767–1778, 2018.

T. W. K. Armitage and A. L. Ridout, “Arctic sea ice freeboard from AltiKa and comparison with CryoSat-2 and Operation IceBridge,” *Geophys. Res. Lett.*, vol. 42, no. 16, pp. 6724–6731, 2015.

N. Besic, G. Vasile, J. Chanussot, S. Stankovic, D. Boldo, and G. D’Urso, “Wet snow backscattering sensitivity on density change for SWE estimation,” Int. Geosci. Remote Sens. Symp., pp. 1174–1177, 2013.

N. Besic, G. Vasile, J. Chanussot, S. Stankovic, J. Dedieu, G. Urso, D. Boldo, J. Ovarlez, C. Grenoble-inp, and D. Tsi, “DRY SNOW BACKSCATTERING SENSITIVITY ON DENSITY CHANGE FOR SWE ESTIMATION University of Montenegro , Podgorica , Montenegro , srdjan@ac.me EDF , R & D STEP , Chatou , France , guy.durso@edf.fr,” pp. 4418–4421, 2012.

Y. Cui, C. Xiong and J. Shi, "Estimation of snow wetness by a dual-frequency radar," *2017 IEEE International Geoscience and Remote Sensing Symposium (IGARSS)*, Fort Worth, TX, 2017, pp. 1363-1365. doi: 10.1109/IGARSS.2017.8127215

Y. Cui, C. Xiong, J. Lemmetyinen, J. Shi, L. Jiang, B. Peng, H. Li, T. Zhao, D. Ji, and T. Hu, “Estimating snow water equivalent with backscattering at X and Ku band based on absorption loss,” *Remote Sens*., vol. 8, no. 6, 2016.

W. Dierking, S. Linow, and W. Rack, “Toward a robust retrieval of snow accumulation over the Antarctic ice sheet using satellite radar,” *J. Geophys. Res. Atmos.,* vol. 117, no. 9, pp. 1–17, 2012.

K.-H. Ding, X. Xu, and L. Tsang, “Electromagnetic Scattering by Bicontinuous Random Microstructures With Discrete Permittivities,” *IEEE Trans. Geosci. Remote Sens.*, vol. 48, no. 8, pp. 3139–3151, Aug. 2010.

M. R. Drinkwater, D. G. Long, and A. W. Bingham, “Greenland snow accumulation estimates from satellite radar scatterometer data,*” J. Geophys. Res. Atmos.*, vol. 106, no. D24, pp. 33935–33950, 2001.

J., Du, J. Shi, and H. Rott (2010), Comparison between a multi-scattering and multi-layer snow scattering model and its parameterized snow backscattering model, Remote Sens. Environ., 114(5), 1089–1098.

J. D., Flach, K. C. Partington, C. Ruiz, E. Jeansou, and M. R. Drinkwater, “Inversion of the surface properties of ice sheets from satellite microwave data”, IEEE Trans. Geosci. Remote Sens.*,43(4), 743–752,doi:10.1109/TGRS.2005.8442. 2005.*

S. Forsström, S. Gerland, and C. A. Pedersen, “Thickness and density of snow-covered sea ice and hydrostatic equilibrium assumption from in situ measurements in Fram Strait, the Barents Sea and the Svalbard coast,” *Ann. Glaciol.*, vol. 52, no. 57 PART 2, pp. 261–270, 2011.

K. Guerreiro, S. Fleury, E. Zakharova, A. Kouraev, F. Rémy, and P. Maisongrande, “Comparison of CryoSat-2 and ENVISAT radar freeboard over Arctic sea ice: toward an improved Envisat freeboard retrieval,” *Cryosph*., vol. 11, 2019.

K. Guerreiro, S. Fleury, E. Zakharova, F. Rémy, and A. Kouraev, “Potential for estimation of snow depth on Arctic sea ice from CryoSat-2 and SARAL/AltiKa missions,” *Remote Sens. Environ.*, vol. 186, pp. 339–349, Dec. 2016.

S. Hendricks, L. Stenseng, V. Helm and C. Haas, "Effects of surface roughness on sea ice freeboard retrieval with an Airborne Ku-Band SAR radar altimeter," *2010 IEEE International Geoscience and Remote Sensing Symposium*, Honolulu, HI, 2010, pp. 3126-3129. doi: 10.1109/IGARSS.2010.5654350

B. Holt, D.R., Johnson M.P., Perkovic-Martin D., and Panzer B., “Snow depth on Arctic sea ice derived from radar: In situ comparisons and time series analysis,” J. *Geophys. Res. Ocean.,* pp. 1–16, 2015.

S., Kern, Khvorostovsky, K., Skourup, H., Rinne, E., Parsakhoo, Z. S., Djepa, V.,Wadhams, P., and Sandven, S., “The impact of snow depth, snow density and ice density on sea ice thickness retrieval from satellite radar altimetry: Results from the ESA-CCI sea ice ECV project round robin exercise”, T*he Cryosphere*, 9, 37–52, https://doi.org/10.5194/tc-9-37-2015, https://www.the-cryosphere.net/9/37/2015/, 2015.

J. King, C. Derksen, P. Toose, A. Langlois, C. Larsen, J. Lemmetyinen, P. Marsh, B. Montpetit, A. Roy, N. Rutter, and M. Sturm, “The influence of snow microstructure on dual-frequency radar measurements in a tundra environment,” *Remote Sens. Environ.*, vol. 215, no. June, pp. 242–254, 2018.

N. T. Kurtz, N. Galin, and M. Studinger, “An improved CryoSat-2 sea ice freeboard retrieval algorithm through the use of waveform fitting,” *Cryosphere*, vol. 8, no. 4, pp. 1217–1237, 2014.

N. T. Kurtz and S. L. Farrell, “Large-scale surveys of snow depth on Arctic sea ice from Operation IceBridge,” Geophys. Res. Lett., vol. 38, no. 20, pp. 1–5, 2011.

R. Kwok, N. T. Kurtz, L. Brucker, A. Ivanoff, T. Newman, S. L. Farrell, J. King, S. Howell, M. A. Webster, J. Paden, C. Leuschen, J. A. MacGregor, J. Richter-Menge, J. Harbeck, and M. Tschudi, "Intercomparison of snow depth retrievals over Arctic sea ice from radar data acquired by Operation IceBridge," *Cryosphere*, vol. 11, no. 6, pp. 2571–2593, 2017.

P. Lacroix, M. Dechambre, B. Legrésy, F. Blarel, and F. Rémy, "On the use of the dual-frequency ENVISAT altimeter to determine snowpack properties of the Antarctic ice sheet," *Remote Sens. Environ.*, vol. 112, no. 4, pp. 1712–1729, 2008.

P. Lacroix, B. Legrésy, R. Coleman, M. Dechambre, and F. Rémy, "Dual-frequency altimeter signal from Envisat on the Amery ice-shelf," *Remote Sens. Environ.*, vol. 109, no. 3, pp. 285–294, 2007.

I. R. Lawrence, M. C. Tsamados, J. C. Stroeve, T. W. K. Armitage, and A. L. Ridout, "Estimating snow depth over Arctic sea ice from calibrated dual-frequency radar freeboards," *Cryosphere*, vol. 12, no. 11, pp. 3551–3564, 2018.

Beno. Legresy and F. Rique Remy, "AltiITletric observations of surface characteristics of the Antarctic ice sheet," 1997.

Y. Lei, P. Siqueira, and R. Treuhaft, "Radio Science A dense medium electromagnetic scattering model for the InSAR correlation of snow."

C. J. Leuschen, R. N. Swift, J. C. Comiso, R. K. Raney, R. D. Chapman, W. B. Krabill, and J. G. Sonntag, "Combination of laser and radar altimeter height measurements to estimate snow depth during the 2004 antarctic AMSR-E sea ice field campaign," *J. Geophys. Res. Ocean.,* vol. 113, no. 4, pp. 1–10, 2008.

C. Leuschen, S. Clifford, and P. Gogineni, "Simulation of a surface-penetrating radar for Mars exploration," J. Geophys. Res, vol. 108, no. E4, p

Z. Li, Z. Li, B. Tian, and J. Zhou, "An InSAR scattering model for multi-layer snow based on Quasi-Crystalline Approximation (QCA) theory," *Sci. China Earth Sci.*, vol. 61, no. 8, pp. 1112–1126, Aug. 2018.

D. Liang, L. Tsang, S. Yueh, and X. Xu, "Modeling active microwave remote sensing of multilayer dry snow using dense media radiative transfer theory," *Int. Geosci. Remote Sens. Symp.*, vol. 3, no. 1, pp. 990–1004, 2008.

D. Liang, X. Xu, K. M. Andreadis, E. G. Josberger, , and L. Tsang, "The Effects of Layers in Dry Snow on Its Passive Microwave Emissions Using Dense Media Radiative Transfer Theory Based on the Quasicrystalline Approximation (QCA/DMRT)", *IEEE T. Geosci. Remote,* 46, 3663–3671, doi:10.1109/TGRS.2008.922143, 2008.

L. Liao, R. Meneghini, A. Tokay, and L. F. Bliven, "Retrieval of snow properties for Ku- and Ka-band dual-frequency radar," *J. Appl. Meteorol. Climatol.*, vol. 55, no. 9, pp. 1845–1858, 2016.

N. Longepe, S. Allain, L. Ferro-Famil, E. Pottier, and Y. Durand, "Snowpack characterization in mountainous regions using c-band sar data and a meteorological model," Geoscience and Remote Sensing, IEEE Transactions on, vol. 47, no. 2, pp. 406 – 418, feb. 2009.

X. V. Phan, L. Ferro-Famil, M. Gay, Y. Durand, M. Dumont, S. Morin, S. Allain, G. D'Urso, and A. Girard, "1D-Var multilayer assimilation of X-band SAR data into a detailed snowpack model," *Cryosphere*, vol. 8, no. 5, pp. 1975–1987, 2014.

X.-V. Phan, L. Ferro-Famil, M. Gay, Y. Durand, M. Dumont, S. Allain, and G. D'Urso, "Analysis of snowpack properties and structure from TerraSAR-X data, based on multilayer backscattering and snow evolution modeling approaches," pp. 1–22, 2012.

G. Picard, M. Sandells, and H. Löwe, "SMRT: An active-passive microwave radiative transfer model for snow with multiple microstructure and scattering formulations (v1.0)," *Geosci. Model Dev.*, vol. 11, no. 7, pp. 2763–2788, 2018.

A. Pope, P. Wagner, R. Johnson, J. D. Shutler, J. Baeseman, and L. Newman, "Community review of Southern Ocean satellite data needs," *Antarct. Sci.*, vol. 29, no. 2, pp. 97–138, 2017.

M. Proksch, C. Mätzler, A. Wiesmann, J. Lemmetyinen, M. Schwank, H. Löwe, and M. Schneebeli: MEMLS3&a: Microwave Emission Model of Layered Snowpacks adapted to include backscattering, Geoscientific Model Development, 8, 2611–2626, https://doi.org/10.5194/gmd-8-2611-2015, 2015.

D. Price, I. Soltanzadeh, and W. Rack, "Snow depth uncertainty and its implications on satellite derived Antarctic sea ice thickness," *Cryosph. Discuss.*, no. May, pp. 1–22, 2018.

G. D. Quartly, E. Rinne, M. Passaro, O. B. Andersen, S. Dinardo, S. Fleury, K. Guerreiro, A. Guillot, S. Hendricks, A. A. Kurekin, F. L. Müller, R. Ricker, H. Skourup, and M. Tsamados, "Review of Radar Altimetry Techniques over the Arctic Ocean: Recent Progress and Future Opportunities for Sea Level and Sea Ice Research," *Cryosph. Discuss.*, no. July, pp. 1–51, 2018.

F. Remy, T. Flament, F. Blarel, and J. Benveniste, "Radar altimetry measurements over Antarctic ice sheet: A focus on antenna polarization and change in backscatter problems," *Adv. Sp. Res.*, vol. 50, pp. 998–1006, 2012.

F. Rémy and S. Parouty, "Antarctic ice sheet and radar altimetry: A Review," *Remote Sens.*, vol. 1, no. 4, pp. 1212–1239, 2009.

R. Ricker, S. Hendricks, V. Helm, H. Skourup, and M. Davidson, “Sensitivity of CryoSat-2 Arctic sea-ice freeboard and thickness on radar-waveform interpretation,” *Cryosphere*, vol. 8, no. 4, pp. 1607–1622, 2014.

R. Ricker, S. Hendricks, D. K. Perovich, V. Helm, and R. Gerdes, “Impact of snow accumulation on CryoSat-2 range retrievals over Arctic sea ice: An observational approach with buoy data,” *Geophys. Res. Lett.*, vol. 42, no. 11, pp. 4447–4455, 2015.

J. K. Ridley, and K. C. Partington: “A model of satellite radar altimeter return from ice sheets”, I*nt. J. Remote Sens.,* 9, 601–624, 1988.

D. Schröder, D. L. Feltham, M. Tsamados, A. Ridout, and R. Tilling, “New insight from CryoSat-2 sea ice thickness for sea ice modeling,” *Cryosphere*, vol. 13, no. 1, pp. 125–139, 2019.

J. Shi *et al*., "Snow water equivalent monitoring from dual-frequency scatterometer on WCOM," *2017 IEEE International Geoscience and Remote Sensing Symposium (IGARSS)*, Fort Worth, TX, 2017, pp. 1359-1362. doi: 10.1109/IGARSS.2017.8127214

Y. F. Song, K., X. B. Zhou, “ELECTROMAGNETIC SCATTERING FROM A MULTI- LAYERED SURFACE WITH LOSSY INHOMOGENEOUS DIELECTRIC PROFILES FOR REMOTE SENSING OF SNOW,” vol. 25, no. June, pp. 197–209, 2012.

Storn, R and Price, K, Differential Evolution - a Simple and Efficient Heuristic for Global Optimization over Continuous Spaces, Journal of Global Optimization, 1997, 11, 341 - 359.

R. L. Tilling, A. Ridout, and A. Shepherd, “Estimating Arctic sea ice thickness and volume using CryoSat-2 radar altimeter data,” *Adv. Sp. Res.*, vol. 62, no. 6, pp. 1203–1225, 2018.

R. T. Tonboe, S. Andersen, R. S. Gill, L. Toudal, and P. Ørsted, “The simulated seasonal variability of the Ku-band radar altimeter effective scattering surface depth in sea ice.”, 2006a.

R. T. Tonboe, L. T. Pedersen, C. Haas, R. T. Tonboe, L. T. Pedersen, and C. Haas, “Simulation of the CryoSat-2 satellite radar altimeter sea ice thickness retrieval uncertainty E 2010 CASI 55,” 2010.

Tsang, Leung & Au Kong, Jin & T. Shin, Robert, “Theory of Microwave Remote Sensing”. Wiley-Interscience. New York, 1985

Tsang, L., Pan, J., Liang, D., Li, Z., Cline, D. W., and Tan, Y.: “Modeling active microwave remote sensing of snow using dense media radiative transfer (DMRT) theory with multiple-scattering effects”, *IEEE T. Geosci. Remote,* 45, 990–1004, doi:10.1109/TGRS.2006.888854, 2007

Xu, X., L. Tsang, and S. Yueh, “Electromagnetic models of Co/Cross polarization of bicontinuous/DMRT in radar remote sensing of terrestrial snow at X-and Ku-band for CoReH2O and SCLP applications”, *IEEE J. Sel. Top. Appl. Earth Obs. Remote Sens*., 5(3), 1024–1032, 2012

Xu, X., L. Tsang, W. Chang, and S. Yueh, “DMRT models of bicontinuous media and QCA multiple-sizes for applications to microwave remote sensing of snowpacks”, paper presented at 2014 *IEEE International Geoscience and Remote Sensing Symposium (IGARSS)*, *IEEE*, 2014

J. Yackel, T. Geldsetzer, M. Mahmud, V. Nandan, S. E. L. Howell, R. K. Scharien, and H. M. Lam, “Snow thickness estimation on first-year sea ice from late winter spaceborne scatterometer backscatter variance,” Remote Sens., vol. 11, no. 4, 2019.

FORM-NT-GB-7-1

Appendix B - **References for other sections**

Aublanc J, Moreau T, Thibaut P, Boy F, Rémy F, et al. (2018) Evaluation of SAR altimetry over the antarctic ice sheet from CryoSat-2 acquisitions. Adv Space Res 62: 1307-1323

Boy, F., J-D. Desjonquères, N. Picot, T. Moreau, and M. Raynal 2017, CRYOSAT-2 SAR Mode Over Oceans: Processing Methods, Global Assessment and Benefits, IEEE Trans. Geosci. Remote Sens., 55, 148-158.

Brenner, A. C., Bindschadler, R. A., Thomas, R. H., and Zwally, H. J. 1983, Slope-induced errors in radar altimetry over continental ice sheets, J. Geophys. Res., 88, 1617–1623

Brown G. S., The average impulse response of a rough surface and its applications, IEEE J. Oceanic Eng. 2, pp. 67–74, 1977.

Davis, C. 1993, A surface and volume scattering retracking algorithm for ice sheet altimetry, IEEE Trans. Geosci. Remote Sensing, 31(4), 811-818

Helm, V., Humbert, A., & Miller, H. 2014, Elevation and elevation change of Greenland and Antarctica derived from CryoSat-2, *The Cryosphere*, *8*(4), 1539-1559

Lacroix P., Dechambre M., Legrésy B., Blarel F., and Rémy F., “On the use of the dual-frequency ENVISAT altimeter to determine snowpack properties of the Antarctic ice sheet,” Remote Sens. Environ., vol. 112, no. 4, pp. 1712–1729, 2008.

Legresy B., Papa F., Remy F., Vinay G., van den Bosch M., Zanife O. Z., “ENVISAT radar altimeter measurements over continental surfaces and ice caps using the ICE-2 retracking algorithm”. Remote Sensing of Environment, 95 (2), 150-163. ISSN 0034-4257, 2005

Legresy, B., and F. Remy 1998, Using the temporal variability of satellite radar altimetric observations to map surface properties of the Antarctic ice sheet, J. Glaciol., 44 (147), 197–206

Partington, K., Ridley, J., Rapley, C., & Zwally, H. (1989). Observations of the Surface Properties of the Ice Sheets by Satellite Radar Altimetry. Journal of Glaciology, 35(120), 267-275. doi:10.3189/S0022143000004603

Picard, G., Royer, A., Arnaud, L., and Fily, M.: Influence of meter-scale wind-formed features on the variability of the microwave brightness temperature around Dome C in Antarctica, The Cryosphere, 8, 1105–1119, https://doi.org/10.5194/tc-8-1105-2014, 2014.

Picard G., Sandells M., and Löwe H., “SMRT: An active–passive microwave radiative transfer model for snow with multiple microstructure and scattering formulations (v1.0),” Geosci. Model Dev., vol. 11, no. 7, pp. 2763–2788, 2018.

Remy, F. and Parouty, S. 2009, Antarctic ice sheet and radar altimetry: A Review, Remote Sensing 1, 1212–1239

Remy, F., T. Flament, F. Blarel, and J. Benveniste 2012, Radar altimetry measurements over Antarctic ice sheet: A focus on antenna polarization and change in backscatter problems, Adv. Space Res. 2012, 50, 998–1006

Ridley, J. K. and K. C. Partington 1988, A model of satellite radar altimeter return from ice sheets, Int. J. Remote Sens., 9(4), 601–624

Sandwell, D. T. and Smith, W. H. F.: Slope correction for ocean radar altimetry., Journal of Geodesy, 88, 765–771, doi:10.1007/s00190-014- 0720-1, 2014

Appendix C - Surface elevation biases tables

Density (kg.m-3)	LRM Elevation bias as function of retracking threshold (TFMRA)					
	25%		50%		75%	
	LRM Ku	LRM Ka	LRM Ku	LRM Ka	LRM Ku	LRM Ka
260	+0.07	-0.07	+0.74	+0.09	+2.67	+0.21
320	*-0.03*	*-0.11*	*+0.25*	*+0.07*	*+1.72*	*+0.20*
380	-0.09	-0.12	+0.15	+0.05	+0.86	+0.18

Table 10: Surface elevation biases for three different snowpack density and for 25%, 50% & 75% retracking thresholds, in LRM Ku & Ka bands

Density (kg.m-3)	SAR Elevation bias as function of retracking threshold (TFMRA)					
	25%		50%		75%	
	SAR Ku	SAR Ka	SAR Ku	SAR Ka	SAR Ku	SAR Ka
260	-0.53	-0.22	-0.22	-0.10	-0.07	0.04
320	*-0.54*	*-0.24*	*-0.24*	*-0.13*	*-0.08*	*-0.02*
380	-0.54	-0.24	-0.24	-0.14	-0.09	-0.05

Table 11: Surface elevation biases for three different snowpack density and for 25%, 50% & 75% retracking thresholds, in SAR Ku & Ka bands

Grain radius (µm)	LRM Elevation bias as function of retracking threshold (TFMRA)					
	25%		50%		75%	
	LRM Ku	LRM Ka	LRM Ku	LRM Ka	LRM Ku	LRM Ka
125	-0.15	-0.07	+0.03	+0.12	+0.21	+0.29
225	*-0.03*	*-0.11*	*+0.25*	*+0.07*	*+1.72*	*+0.20*
325	+0.02	-0.15	+0.28	+0.03	+1.15	+0.17

Table 12: Surface elevation biases for three different snow grain size and for 25%, 50% & 75% retracking thresholds, in LRM Ku & Ka bands

Grain radius (µm)	SAR Elevation bias as function of retracking threshold (TFMRA)					
	25%		50%		75%	
	SAR Ku	SAR Ka	SAR Ku	SAR Ka	SAR Ku	SAR Ka
125	-0.55	-0.24	-0.25	-0.13	-0.11	-0.02
225	*-0.54*	*-0.24*	*-0.24*	*-0.13*	*-0.08*	*-0.02*
325	-0.51	-0.25	-0.21	-0.17	-0.04	-0.08

Table 13: Surface elevation biases for three different snow grain size and for 25%, 50% & 75% retracking thresholds, in SAR Ku & Ka bands

mean square slope	LRM Elevation bias as function of retracking threshold (TFMRA)					
	25%		50%		75%	
	LRM Ku	LRM Ka	LRM Ku	LRM Ka	LRM Ku	LRM Ka
0.01	-0.14	-0.15	+0.05	+0.03	+0.24	+0.17
0.03	*-0.03*	*-0.11*	*+0.25*	*+0.07*	*+1.72*	*+0.20*
0.05	+0.07	-0.08	+0.71	+0.08	+2.48	+0.21

Table 14: Surface elevation biases for three different mean square slopes and for 25%, 50% & 75% retracking thresholds, in LRM Ku & Ka bands

mean square slope	SAR Elevation bias as function of retracking threshold (TFMRA)					
	25%		50%		75%	
	SAR Ku	SAR Ka	SAR Ku	SAR Ka	SAR Ku	SAR Ka
0.01	-0.54	-0.25	-0.25	-0.16	-0.10	-0.07
0.03	*-0.54*	*-0.24*	*-0.24*	*-0.13*	*-0.08*	*-0.02*
0.05	-0.53	-0.23	-0.23	-0.11	-0.06	+0.02

Table 15: Surface elevation biases for three different mean square slopes and for 25%, 50% & 75% retracking thresholds, in SAR Ku & Ka bands